

Molecular Properties by Quantum Monte Carlo: An Investigation on the Role of the Wave Function Ansatz and the Basis Set in the Water Molecule

Andrea Zen,[†] Ye Luo,[‡] Sandro Sorella,^{*,‡} and Leonardo Guidoni^{*,§}

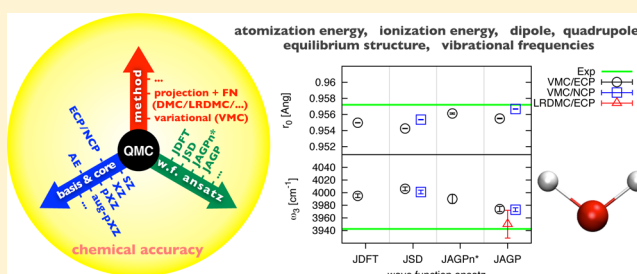
[†]Dipartimento di Fisica, La Sapienza—Università di Roma, Piazzale Aldo Moro 2, 00185 Rome, Italy

[‡]Scuola Internazionale Superiore di Studi Avanzati (SISSA), via Bonomea 265, 34136 Trieste, Italy

[§]Dipartimento di Scienze Fisiche e Chimiche, Università degli studi de L'Aquila, Via Vetoio, 67100 Coppito, L'Aquila, Italy

S Supporting Information

ABSTRACT: Quantum Monte Carlo methods are accurate and promising many body techniques for electronic structure calculations which, in the last years, are encountering a growing interest thanks to their favorable scaling with the system size and their efficient parallelization, particularly suited for the modern high performance computing facilities. The ansatz of the wave function and its variational flexibility are crucial points for both the accurate description of molecular properties and the capabilities of the method to tackle large systems. In this paper, we extensively analyze, using different variational ansatzes, several properties of the water molecule, namely, the total energy, the dipole and quadrupole momenta, the ionization and atomization energies, the equilibrium configuration, and the harmonic and fundamental frequencies of vibration. The investigation mainly focuses on variational Monte Carlo calculations, although several lattice regularized diffusion Monte Carlo calculations are also reported. Through a systematic study, we provide a useful guide to the choice of the wave function, the pseudopotential, and the basis set for QMC calculations. We also introduce a new method for the computation of forces with finite variance on open systems and a new strategy for the definition of the atomic orbitals involved in the Jastrow-Antisymmetrised Geminal power wave function, in order to drastically reduce the number of variational parameters. This scheme significantly improves the efficiency of QMC energy minimization in case of large basis sets.



1. INTRODUCTION

Quantum Monte Carlo^{1–4} (QMC) stands for a number of different stochastic methods that are used for electronic structure calculations of solids and molecules. These techniques range from the simplest and computationally cheapest variational Monte Carlo (VMC) scheme, to the more sophisticated and computationally expensive projection methods, such as the diffusion Monte Carlo^{5–8} (DMC), the Green function Monte Carlo^{9–12} (GFMC), the lattice regularized diffusion Monte Carlo^{13,14} (LRDMC), the auxiliary field quantum Monte Carlo^{15–17} (AFQMC), the released node quantum Monte Carlo,^{18,19} the self-healing diffusion Monte Carlo²⁰ (SHDMC), the reptation quantum Monte Carlo^{21,22} (RQMC), or the recent full configuration interaction Quantum Monte Carlo²³ (FCI-QMC). In recent years, the QMC methods are encountering a growing interest due to the favorable scaling of the algorithms with the system size²⁴ (the computational cost scales with the number N of electrons as N^m with m between 3 and 4), an accuracy comparable to those of other high-level correlated quantum chemistry methods,^{25–35} and their readiness for the implementation in modern highly parallel supercomputer facilities.²⁴

Despite QMC techniques have been known for more than three decades, their application has been quite limited if compared to other methods, such as Density Functional Theory (DFT), or traditional quantum chemistry methods, such as coupled-cluster³⁶ (CC), configuration interaction³⁷ (CI), Møller–Plesset perturbation theory,^{38,39} and Complete Active Space Self-Consistent Field (CASSCF). Due to the large computational cost, the use of QMC has been often restricted to particularly challenging systems, especially those characterized by the presence of strong electron correlation. This is probably due to the underlying stochastic nature of QMC that, on one side, it is responsible for the favorable scaling with the number of electrons and the intrinsic parallelization but, on the other side, it yields expectation values $\langle O \rangle$ of any operator O affected by an associated stochastic error σ_O , converging to zero quite slowly, namely like the inverse square root of the computational time. Since this scaling has usually a large prefactor, the stochastic error affecting QMC calculations is typically much larger than the corresponding numerical errors affecting nonstochastic computational methods.

Received: May 10, 2013

Published: August 28, 2013



Strictly connected with such underlying stochastic error of QMC is the “historical” challenge to calculate reliable ionic forces. The straightforward employment of the finite difference methods is quite inefficient, due to the propagation of the stochastic errors when energy differences are considered. However, a number of technical improvements have significantly reduced these problems, making possible to realize calculations of increasing complexity with an affordable computational cost. The introduction of the correlated sampling⁴⁰ (CS) and the space warp coordinate transformation⁴¹ (SWCT) lead to large improvements in calculating energy differences between two different wave functions, and then on the force evaluation. Anyway, the finite difference approaches have a computational cost proportional to 3 times the number of atoms, making it prohibitive for large molecules. Concerning the analytical approaches for the calculation of the forces, large improvements have been achieved by the introduction of the reweighting methods for the stochastic sampling,^{42–44} which allows us to overcome the well-known problem of the infinite variance of the force estimators. A further step in the direction of an efficient and accurate computation of the QMC forces has been recently accomplished by Sorella and Capriotti,⁴⁵ who proposed a combined use of the reweighting method, the CS, and the SWCT techniques. Thanks to the use of the algorithmic adjoint differentiation (AAD), all the components of the ionic forces are calculated in a computational time that is only about four times the one of an ordinary energy calculation, in both the cases of all electrons and pseudopotential calculations. Thanks to these improvements in the force evaluations, in the last years several optimizations of molecular geometries, based on QMC calculations, have been reported,^{24,25,45–49} for molecules of growing size and complexity. Another important issue emerging from recent QMC literature is the possibility to calculate ground state molecular properties beyond energies and geometries, such as, for instance, the polarizability and the electronic density.^{3,50} Recently, by using a procedure based on the multidimensional fitting of the potential energy surface (PES) of a molecule in proximity of its configurational minimum, it has also been shown that it is possible to calculate the harmonic vibrational frequencies and the anharmonic corrections by QMC, despite the presence of stochastic errors.⁵¹

Another area in which the QMC has recently undergone a remarkable progress is the introduction and the characterization of several new wave function ansatzes. The wave function variational ansatz is, indeed, of fundamental importance for the accuracy and the reliability of both variational and diffusion Monte Carlo results, as it emerges from different works.^{25,48,50,52–55} As expected, the definition of the wave function is more important for the VMC technique rather than for the corresponding DMC projection method, since the latter only depends on the nodal surface of the variational wave function. A typical QMC wave function is given by an antisymmetric determinantal part, aimed to describe static correlation effects, and a bosonic part, termed the Jastrow factor,⁵⁶ which recovers most of the dynamical correlation effects. Going beyond the simplest wave function where to a single Slater determinant is applied a Jastrow term, among recent wave function developments we can include the Jastrow antisymmetrized geminal power (JAGP) wave function,⁵⁷ the Pfaffian wave function,^{58,59} wave functions with backflow correction,⁶⁰ and many other multideterminant Jastrow functions.^{53,54,61,62} The JAGP is a particularly interesting and promising ansatz, due to its ability to represent a multideterminant

wave function in an implicit and compact way. Moreover, the presence of the Jastrow factor allows to satisfy the size consistency that, as observed in ref 33 and more recently by Neuscamman,⁶³ is not fulfilled by the simple AGP ansatz.

In many papers, convergence studies have been carried out as a function of the basis set size.^{32,33,50,64,65} An emerging trend is that the optimization of all wave function parameters, including the coefficients of the contractions and the exponents of the primitive gaussians, can accelerate the convergence of many observables. As expected, different observables (such as geometries, energies, polarizabilities and vibrational frequencies) have a different convergence behavior with respect to the size of the basis set and the number and kind of parameters to be optimized, as pointed out for instance by Coccia et al. in the case of the ethyne polarizability.⁵⁰

In QMC, the interplay between the variational ansatz and the basis set size is quite intricate and not yet completely understood. The number of variational parameters is also a crucial issue for the QMC wave function optimization, since it grows both with the wave function complexity and the size of the basis set. Also, the kind of variational parameter (linear or nonlinear) can be important for the practical stability of the wave function optimization algorithms.

In order to investigate systematically the behavior of the different variational ansatzes, together with the choice of the basis sets for the determinantal and the Jastrow part of the wave function, in the present work we propose an extensive study of the molecular properties of the water molecule, both with all electron wave functions and pseudopotentials. The investigation mainly focuses on the VMC scheme, although several LRDMC calculations are also reported. We have considered as a test case the water molecule, because it is a sufficiently small system to afford different calculations of several properties, but it still preserves a certain degree of complexity, allowing a meaningful application of the various approaches. Moreover, the water molecule has been widely studied and characterized both experimentally^{66–68} and by using highly accurate *ab initio* computational approaches,^{69–75} which provide useful benchmarks for our QMC calculations. The accuracy of the different approaches has been tested versus a number of different properties, namely the energy, the dipole, the quadrupole, the ionization and atomization energies, the structural minimum, and the harmonic and the fundamental frequencies of vibration. In addition to this systematic study, we introduce in the present paper a new scheme of building the atomic orbitals involved in the wave functions, called hereafter *atomic hybrid orbitals*. Due to the tight relationships between the variational parameters and the basis sets, the proposed scheme would be particularly suitable and computationally convenient in the treatments of large systems with large basis sets.

The paper includes a self-contained description of the used wave function ansatzes in Section 2, and of the QMC techniques in Section 3. In these sections some novel methodological improvements are also presented. Together with the new hybrid orbitals, we also provide an improvement for open nonperiodic systems of the *reweighting method* proposed by Attaccalite and Sorella.⁴⁴ In Section 4, we provide some additional details about the computation that we have performed, that are reported and discussed in Section 5, followed by a conclusive discussion in Section 6 of the impact of the work and of the future perspectives.

2. FUNCTIONAL FORM OF THE QMC WAVE FUNCTION

The usual form of a QMC wave function⁴ is the product of an antisymmetric (fermionic) function Ψ_A and a symmetric (bosonic) exponential function $J = e^U$:

$$\Psi_{\text{QMC}}(\bar{\mathbf{x}}) = \Psi_A(\bar{\mathbf{x}})J(\bar{\mathbf{x}}) \quad (1)$$

Both Ψ_A and J , hereafter called respectively the *determinantal part* and the *Jastrow factor* of the wave function, depend on the spatial \mathbf{r}_i and spin σ_i coordinates of the N electrons in the system, being $\bar{\mathbf{x}} = \{\mathbf{x}_i\}_{i=1,\dots,N}$ and $\mathbf{x}_i = (\mathbf{r}_i, \sigma_i)$. The determinantal part Ψ_A , sum of one or more Slater determinants, completely defines the nodal surface of Ψ_{QMC} , and it is responsible for the description of the static correlation. The Jastrow factor, explicitly dependent on the interelectronic distances, describes the dynamical correlation between the electrons and is used also to satisfy the cusp conditions.^{4,76}

Ψ_{QMC} , as well as its constituting determinantal and Jastrow parts, is functionally dependent on some parameters, that are optimized in order to minimize the corresponding variational energy. The optimized wave function should provide the best description of the electronic properties, and of the static and dynamical correlation, within the limitations of the considered ansatz. However, when the number of variational parameters of the wave function increases, their optimization can become very challenging. It is therefore crucial to adopt a parametric wave function that has a large variational flexibility but, at the same time, a limited number of tunable parameters.

In the next paragraph, we will provide a synthetic description of the atomic orbitals that are used in the determinantal and the Jastrow parts of the wave function. Next, we will review the different forms for the determinantal part Ψ_A that are considered in this work, namely the Antisymmetrized Geminal Power (AGP), the single Slater Determinant (SD), and the AGP with fixed number of molecular orbitals (AGPn*). Afterward we will provide a description of the Jastrow factor.

2.1. Atomic Orbitals. The choice of the primitive atomic orbitals and the contractions is important to achieve a rapid basis set convergence (BSC) and balanced calculations, both for QMC and for many other electronic structure methods. However in QMC calculations, at variance with other techniques, all the basis set parameters (included the exponents and the contraction coefficients) are often optimized during the minimization of the variational energy. An appropriate choice for the contraction scheme is particularly important in the AGP wave function, since for this wave function the atomic orbital contractions and the number of wave function parameters are closely related, as we will see in Section 2.2.

A generic atomic orbital $\phi_{\mu_a}^a(\mathbf{r}_{ia})$ of the atom a is written in terms of the radial vector $\mathbf{r}_{ia} = \mathbf{r}_i - \mathbf{R}_a$ connecting the nucleus of the atom a with the position \mathbf{r}_i of the electron i . In this work we will consider three different types of atomic orbitals: (i) the *uncontracted orbitals*, (ii) the *contracted orbitals*, and (iii) the *contracted atomic hybrid orbitals*.

An uncontracted orbital $\phi_{l,m}$, having azimuthal quantum number l and magnetic quantum number m , is the product of an angular part, that is, real spherical harmonic, and a radial part. The latter may have several functional forms; in this work, we have considered only the two most used: the Slater type orbitals (STO)

$$\phi_{l,m}^{\text{STO}}(\mathbf{r}; \zeta) \propto r^l e^{-\zeta r} Z_{l,m}(\Omega) \quad (2)$$

and the Gaussian type orbitals (GTO)

$$\phi_{l,m}^{\text{GTO}}(\mathbf{r}; \zeta) \propto r^l e^{-\zeta r^2} Z_{l,m}(\Omega) \quad (3)$$

where $Z_{l,m}(\Omega)$ is the real spherical harmonic and $r = \|\mathbf{r}\|$. The proportionality constant is fixed by the normalization and depends on the parameter ζ . Other parametric forms for the atomic orbitals exist, see for instance Petruziello et al.,⁶⁴ but are not used in this work.

In our implementation, the nuclear cusp condition is satisfied by an electron–nucleus interaction term that is included in the Jastrow factor. For this reason, we need atomic orbitals with no cusps at the nuclei. This is automatically satisfied by all the GTO and STO orbitals in eqs 2 and 3, with the exception of the STO orbital s (i.e., $l = m = 0$). For this reason, the latter orbital is replaced by the following:

$$\phi_{0,0}^{\text{STO}}(\mathbf{r}; \zeta) \propto (1 + \zeta r) e^{-\zeta r} \quad (4)$$

Each of the uncontracted orbitals described above depends parametrically only on the value of the ζ in the exponent.

The contracted orbitals $\phi_{l,m}^K$ are simple generalizations of the uncontracted orbitals, where the radial part is the summation of the radial parts of several uncontracted orbitals (GTOs, STOs, or mixed). Therefore, a contracted orbital is

$$\phi_{l,m}^K(\mathbf{r}; \{\zeta_k, c_k\}) = \sum_{k=1}^K c_k \phi_{l,m}^{X_k}(\mathbf{r}, \zeta_k) \quad (5)$$

where X_k can be GTO or STO and K is the number of summed uncontracted orbitals. The number of variational parameters in $\phi_{l,m}^K$ is $2K - 1$, given by the K exponents and the K coefficients, minus one due to the overall normalization of the orbital.

In this work, we have introduced and tested another type of contracted orbital, hereafter indicated with the name of *atomic hybrid orbital*. It represents a further “drastic” generalization of the contraction of an orbital that is rather similar to the well-known expansion in natural hybrid orbitals.⁷⁷ It is written in the following way:

$$\phi_a(\mathbf{r}; \{\zeta_{k,l}, c_{l,m}^k\}) = \sum_{l=0}^{l_{\text{MAX}}} \sum_{k=1}^{K_l} \sum_{m=-l}^{+l} c_{l,m}^k \phi_{l,m}^{X_{k,l}}(\mathbf{r}, \zeta_{k,l}) Z_{l,m}(\Omega) \quad (6)$$

The number of parameters here is given by the sum of the number of exponents and of the coefficients. The number of exponents $\{\zeta_{k,l}\}$ is given by $n_z = \sum_{l=0}^{l_{\text{MAX}}} n_z^l$, being n_z^l the number of exponents with angular momentum l . The number of coefficients $\{c_{l,m}^k\}$ is $n_c = \sum_{l=0}^{l_{\text{MAX}}} (2l + 1) * n_z^l - 1$, the minus one being introduced for the normalization. An atomic hybrid orbital ϕ_a , related to the atom a , is written as the sum of all the uncontracted orbitals, of any azimuthal and magnetic quantum numbers, that we want to use to describe the atom. For the description of an atom, it is generally required to use more than one atomic hybrid orbital (the number of which will be in the following indicated between brace parentheses). Both the exponents and the coefficients have to be conveniently optimized, and in principle, they can be different (especially the coefficients) even for different atoms of the same type appearing in the same molecule.

These atomic hybrid orbitals somehow remind the well-known natural orbitals,⁷⁷ but differently from natural orbitals, our hybrid orbitals are not necessarily orthonormal and are obtained by straightforward optimization of the energy.

2.2. AGP Wave Function. The Antisymmetrized Geminal Power is a particular pairing wave function that describes the correlations between pairs of electrons by means of a two-particle

geminal function. Initially introduced to describe spin unpolarized systems,⁷⁸ it has been generalized in order to describe also spin polarized systems, i.e., systems with unpaired electrons.^{57,79} Hereafter, we limit our description to the case of spin unpolarized systems, and we refer to the work of Casula and Sorella⁵⁷ for the generalization to spin polarized systems.

A spin unpolarized system, with zero total spin, has the number N^\uparrow of electrons with spin up equal to the number N^\downarrow of electrons with spin down and to one-half of the total number of electrons N . In this case the AGP wave function is

$$\Psi_{\text{AGP}}(\bar{\mathbf{x}}) = \hat{A}[G(\mathbf{x}_1; \mathbf{x}_2)G(\mathbf{x}_3; \mathbf{x}_4)\cdots G(\mathbf{x}_{N-1}; \mathbf{x}_N)] \quad (7)$$

where \hat{A} is the antisymmetric operator, and $G(\mathbf{x}_i; \mathbf{x}_j)$ is the geminal function, a product of a spin singlet and a symmetric spatial wave function $g(\mathbf{r}_i; \mathbf{r}_j)$:

$$G(\mathbf{x}_i; \mathbf{x}_j) = g(\mathbf{r}_i; \mathbf{r}_j) \frac{\delta(\sigma_i, \uparrow)\delta(\sigma_j, \downarrow) - \delta(\sigma_i, \downarrow)\delta(\sigma_j, \uparrow)}{\sqrt{2}} \quad (8)$$

It can be shown⁵⁷ that the spatial part of Ψ_{AGP} can be written as the determinant of a matrix $\mathbf{M}_{ij}^{\text{AGP}}$ of dimension $N/2 \times N/2$ whose elements are $M_{ij}^{\text{AGP}} = (r_i, r_{N/2+j})$, with $i, j = 1, \dots, N/2$.

The spatial geminal function g is written in terms of single electron atomic wave functions:

$$g(\mathbf{r}_i; \mathbf{r}_j) = \sum_{a,b} \sum_{\mu_a} \sum_{\mu_b} \lambda_{\mu_a \mu_b}^{a,b} \phi_{\mu_a}^a(\mathbf{r}_{ia}) \phi_{\mu_b}^b(\mathbf{r}_{jb}) \quad (9)$$

where a and b are the atom indexes, running from 1 to the number M of atoms in the system, and μ_a labels the L_a local atomic orbitals $\phi_{\mu_a}^a$ used to describe the atom a . The local orbital $\phi_{\mu_a}^a$ is a function of the difference $\mathbf{r}_{ia} = \mathbf{r}_i - \mathbf{R}_a$ between the position \mathbf{r}_i of the electron i and the position \mathbf{R}_a of the nucleus a . The $\lambda_{\mu_a \mu_b}^{a,b}$ coefficients in eq 9 represent the weight of the superposition of different orbitals, analogously to the valence bond representation, or in other words the contribution of the atomic orbital μ_a of the atom a and the atomic orbital μ_b of the atom b to the formation of the chemical bond between a and b . The set of coefficients $\lambda_{\mu_a \mu_b}^{a,b}$ defines the square matrix Λ of size $L \times L$, where $L = \sum_a L_a$ is the total number of atomic orbitals defining our basis set. In order to ensure that the total spin is conserved, the condition $\lambda_{\mu_a \mu_b}^{a,b} = \lambda_{\mu_b \mu_a}^{b,a}$ is required, that is, the Λ matrix is symmetric. This implies that the number of independent parameters in the Λ matrix is $L(L+1)/2$. Moreover, if molecular symmetries are present, it is possible to introduce additional constraints on the elements of the Λ matrix, that can significantly reduce the number of independent parameters of the wave function.⁸⁰

In the following sections, we will consider other functional forms for the determinantal part of the wave function. The relation between the AGP and those other wave functions can be easily understood by rewriting the pairing function $g(\mathbf{r}_i; \mathbf{r}_j)$ in an equivalent way, where the Λ matrix is diagonalized. In order to diagonalize Λ , it is convenient to take into account that the atomic orbitals are not necessarily orthogonal each other, namely the overlap matrix $S_{\mu_a \mu_b}^{a,b} \equiv \langle \phi_{\mu_a}^a | \phi_{\mu_b}^b \rangle \neq 1$, and by using a standard generalized diagonalization:

$$\Lambda \mathbf{S} \mathbf{P} = \mathbf{P} \bar{\Lambda} \quad (10)$$

In eq 10, each column of the matrix \mathbf{P} represents a generalized eigenvector of Λ , and the corresponding eigenvalues $\bar{\lambda}_\alpha$

constitute the elements of the diagonal matrix $\bar{\Lambda} = \text{diag}(\bar{\lambda}_1, \dots, \bar{\lambda}_L)$, sorted in decreasing order of their absolute value: $|\bar{\lambda}_1| \geq |\bar{\lambda}_2| \geq \dots \geq |\bar{\lambda}_L| \geq 0$. Thus, from $\mathbf{P}^T \mathbf{S} \mathbf{P} = \mathbf{I}$, by right multiplying both sides of eq 10 for the matrix $\mathbf{P}^T = (\mathbf{S} \mathbf{P})^{-1}$ we obtain $\Lambda = \mathbf{P} \Lambda \mathbf{P}^T$. Then, by substituting it in eq 9, we finally obtain that the pairing function is

$$g(\mathbf{r}_i; \mathbf{r}_j) = \sum_{\alpha=1}^L \bar{\lambda}_\alpha \Phi_\alpha(\mathbf{r}_i) \Phi_\alpha(\mathbf{r}_j) \quad (11)$$

where we have defined the orthogonal single particle orbitals:

$$\Phi_\alpha(\mathbf{r}_i) = \sum_a \sum_{\mu_a} P_\alpha^{a,\mu_a} \phi_{\mu_a}^a(\mathbf{r}_{ia}) \quad (12)$$

which will be afterward named molecular orbitals (MOs). The complete basis set (CBS) for the pairing function in eq 11 is reached in the limit $L \rightarrow \infty$, namely in the limit of considering an infinite number of MOs.

2.3. SD Wave Function. It can be reasonably expected that the leading terms in the expansion of the pairing function g in eq 11 are provided by a limited set of MOs associated to the eigenvalues $\bar{\lambda}_\alpha$ largest in absolute value $|\bar{\lambda}_\alpha|$. Therefore, by considering a truncated pairing function, where only a subset $n \ll L$ of the MOs are used instead of all the L orbitals appearing in eq 11, we have that, if n is large enough to provide the leading behavior of g , the quality of the parametrical wave function is not significantly affected. This truncation substantially reduce the number of variational parameters (working with a $n \times L$ matrix instead of the larger $L \times L$ matrix Λ).

The lowest number of orbitals that we have to consider to describe an unpolarized system of N electrons is exactly equal to the number of electron pairs $N/2$. Thus, within this minimal approach, the pairing function is

$$g^{\text{SD}}(\mathbf{r}_i; \mathbf{r}_j) = \sum_{\alpha=1}^{N/2} \bar{\lambda}_\alpha \Phi_\alpha(\mathbf{r}_i) \Phi_\alpha(\mathbf{r}_j) \quad (13)$$

It can be seen that the antisymmetrization operator in eq 7, applied to the truncated pairing function in eq 13, singles out only one Slater determinant (SD); therefore, hereafter, this wave function will be referred as the SD function. We also observe that the MO weights $\bar{\lambda}_\alpha$ affect only the overall pre factor of this Slater determinant, so that their actual values are irrelevant in this case. This SD function is the equivalent of a restricted Hartree–Fock (RHF) function, in HF calculations, or of a restricted Kohn–Sham function, in DFT calculations. However, within a QMC scheme, a Jastrow factor is always introduced in the wave function, in order to enhance the description of the dynamical correlations between the electrons. When a Jastrow factor, of the type that will be described in Section 2.5, is applied to a SD function, it will be referred as Jastrow correlated single determinant (JSD) function.

It has been observed in several cases^{4,57,65} that a JSD wave function is able to describe the atoms with an high level of accuracy. However, for several molecular systems the JSD function is unable to provide an equally accurate and reliable description of several properties. For these cases, the JAGP function results to provide a much more accurate description. An important property to be considered for a reliable description of a molecular system is whether the wave function is size consistent. The JAGP is size consistent^{33,63} in all cases where the JSD is size consistent, namely when the spin/angular momentum of the compound is the sum of the spin/angular momentum of the

fragments. A remarkable exception is when the fragments are $S = 1/2$ atoms, such as the H_2 and F_2 , where the JAGP is size consistent and the JSD is not. In addition to this, there are several other reasons to use the JAGP rather than a simpler JSD:

- It is more accurate at a similar computational cost.
- It is a more compact representation of the determinantal part within a localized atomic basis, thus it is simple to implement constraints which avoid to optimize variationally irrelevant parameters. For instance the symmetries, such as the translation, can be simply implemented as constraints in the Λ matrix.
- For large systems, a big reduction of the variational freedom is possible by disregarding matrix elements of Λ corresponding to localized orbitals very far in space.

2.4. AGPn* Wave Function. In order to improve upon the simple JSD wave function for a more accurate description of molecules, we have to include in the pairing function g a number n of MOs larger than $N/2$, $n = N/2$ corresponding to the JSD function. Since a JSD function provides an accurate description of the atoms, a natural criterium for the choice of the number of MOs is by requiring that, when the atoms are at large distances, we cannot obtain an energy below the sum of the JSD atomic energies. The number n^* of MOs defined in this way is determined by the requirement that

$$n^* \leq \sum_a^M N^\uparrow(A_a) + m - 1 \quad (14)$$

where A_1, \dots, A_M identify the M atoms forming the system, $N^\uparrow(A_a)$ is the number of spin up electrons for a description of the atom A_a , and m is equal to the minimum number of identical atoms in the system (for further details and for a discussion of the case of polarized systems see Marchi et al.⁶⁵).

Therefore, the pairing function associated to n^* is defined as

$$g^{n^*}(\mathbf{r}_i, \mathbf{r}_j) = \sum_{\alpha=1}^{n^*} \bar{\lambda}_\alpha \Phi_\alpha(\mathbf{r}_i) \Phi_\alpha(\mathbf{r}_j) \quad (15)$$

The Jastrow correlated AGP function obtained by the antisymmetrization of the geminal g^{n^*} will be hereafter indicated with JAGPn*.⁶⁵

2.5. The Jastrow Factor. The bosonic Jastrow term, $J = e^U$, represents a compact and efficient way to introduce explicitly the electronic correlation in the wave function, because it depends directly on distances between electrons. Several different implementations of the Jastrow term are used in the QMC codes. The Jastrow that we have used in this work consists of several terms that account for the 2-body, 3-body, and 4-body interaction between the electrons and the nuclei. The exponent U of the Jastrow factor can therefore be conveniently written as the sum of three independent functions:

$$U = U_{en} + U_{ee} + U_{een[n]} \quad (16)$$

The leading contribution is given by $U_{ee}(\bar{\mathbf{r}})$, that is a homogeneous *two electron* interaction term. It depends only on the relative distance between pairs of electrons, and it improves the electron–electron correlation, besides satisfying the electron–electron cusp condition for unlike spin. The cusp condition for like spin is not satisfied, as this would lead to spin contamination.^{57,81} However, this is a minor problem because the probability for like spin electrons to be close is very small, because of the Pauli principle. The functional form that we have used for U_{ee} is

$$U_{ee}(\bar{\mathbf{r}}) = \sum_{i < j}^N u_2(r_{ij}) \quad (17)$$

where $r_{ij} = \|\mathbf{r}_i - \mathbf{r}_j\|$ is the distance between electrons i and j , and $u_2(x) = (1 - e^{-b_2 x})/(2b_2)$ is a function of the variational parameter b_2 .

The term U_{en} is a *one electron* interaction term which improves the electron–nucleus correlation and satisfies the nuclear cusp condition. Its functional form is

$$U_{en}(\bar{\mathbf{r}}, \bar{\mathbf{R}}) = - \sum_a^M [(2Z_a)^{3/4} \sum_i^N u_1(\sqrt{2Z_a} r_{ia})] + \sum_a^M \sum_{\nu_a}^{L_a^J} [\sum_i^N f_{\nu_a}^a \chi_{\nu_a}^a(\mathbf{r}_{ia})] \quad (18)$$

where the vector $\mathbf{r}_{ia} = \mathbf{r}_i - \mathbf{R}_a$ is the difference between the position of the nucleus a and the electron i , $r_{ia} = \|\mathbf{r}_{ia}\|$ is their distance, Z_a is the electronic charge of the nucleus a , L_a^J is the number of atomic orbitals $\chi_{\nu_a}^a$ that are used to describe the atom a (they are similar to the $\phi_{\mu_a}^a$ orbitals used for the determinantal part), $f_{\nu_a}^a$ are variational parameters and the function $u_1(x) = (1 - e^{-b_1 x})/(2b_1)$ is used to satisfy the electron–nucleus cusp condition, and it depends parametrically on the value of b_1 .

The term $U_{een[n]}$ is an inhomogeneous *two electron* interaction term, and it has the following form:

$$U_{een[n]}(\bar{\mathbf{r}}, \bar{\mathbf{R}}) = \sum_{i < j}^N [\sum_{a,b}^M \sum_{\nu_a}^{L_a^J} \sum_{\nu_b}^{L_b^J} f_{\nu_a, \nu_b}^{a,b} \chi_{\nu_a}^a(\mathbf{r}_{ia}) \chi_{\nu_b}^b(\mathbf{r}_{jb})] \quad (19)$$

where the $\chi_{\mu_a}^a$ are the same atomic orbitals that appear also in U_{ee} , second term in the right-hand side of eq 18, and $f_{\nu_a, \nu_b}^{a,b}$ are variational parameters. In eq 19 are included both the three body *e-e-n* interactions and the four body *e-e-n-n* interactions, for $a = b$ and for $a \neq b$, respectively.

3. QUANTUM MONTE CARLO METHODS

The expectation value of an observable O , with corresponding quantum mechanical operator \hat{O} , is evaluated as $\langle O \rangle \equiv \langle \psi | \hat{O} | \psi \rangle / \langle \psi | \psi \rangle$, involving the computation of $3N$ -dimensional integrals. Differently from HF or post-HF approaches, with QMC wave functions these integrals do not factorize, due to the presence of the Jastrow factor. In Section 3.1, we review some aspects about the stochastic approach adopted to evaluate these integrals within VMC. In Section 3.2, we discuss the specific case of the energy evaluation, in Section 3.3 the variational optimization of the wave function parameters, in Section 3.4 the force evaluation, and in Section 3.5 the reweighting technique used to have a well behaved expectation value of the force for open systems (namely, having finite variance). Next, in Section 3.6, we discuss the dipole and quadrupole evaluations. Finally, in Section 3.7, we briefly review some aspects of the projection Monte Carlo approaches.

3.1. Stochastic Evaluation of the Expectation Value of an Observable. VMC is a stochastic method for the estimation of the expectation value $\langle O \rangle$ associated to a parametric wave function ψ . The method is based on the fact that any expectation value $\langle O \rangle$ can be rewritten as

$$\langle O \rangle = \frac{\langle O_L(\bar{\mathbf{x}}) \psi(\bar{\mathbf{x}})^2 / W(\bar{\mathbf{x}}) \rangle_{P(\bar{\mathbf{x}})}}{\langle \psi(\bar{\mathbf{x}})^2 / W(\bar{\mathbf{x}}) \rangle_{P(\bar{\mathbf{x}})}} \quad (20)$$

where $O_L(\bar{\mathbf{x}}) \equiv \psi(\bar{\mathbf{x}})^{-1} \hat{O} \psi(\bar{\mathbf{x}})$ is the so-called *local value* of the operator \hat{O} calculated in the specific electronic configuration $\bar{\mathbf{x}}$, $P(\bar{\mathbf{x}})$ is an appropriately chosen probability density distribution determined by a known positive weight $W(\bar{\mathbf{x}})$ up to a normalization constant, namely $P(\bar{\mathbf{x}}) = W(\bar{\mathbf{x}}) / \int W(\bar{\mathbf{x}}) d\bar{\mathbf{x}}$ and $\langle f(\bar{\mathbf{x}}) / W(\bar{\mathbf{x}}) \rangle_{P(\bar{\mathbf{x}})}$ represents the expectation value $E[f]$ of a function $f(\bar{\mathbf{x}})$ that is calculated by sampling over a probability distribution $P(\bar{\mathbf{x}})$ the function $f(\bar{\mathbf{x}}) / W(\bar{\mathbf{x}})$. The most common and simple choice for the positive weight W is $W(\bar{\mathbf{x}}) = \psi(\bar{\mathbf{x}})^2$, in which case the denominator in eq 20 is identically one and the expression for $\langle O \rangle$ simplifies in

$$\langle O \rangle = \langle O_L(\bar{\mathbf{x}}) \rangle_{\Pi(\bar{\mathbf{x}})} \quad (21)$$

which is usually referred as *standard sampling*. Notice that in quantum Monte Carlo it is not necessary to know the rather involved normalization constant $\int W(\bar{\mathbf{x}}) d\bar{\mathbf{x}}$ to generate configurations according to the probability distribution $P(\bar{\mathbf{x}})$. Only weight ratios $W(\bar{\mathbf{x}}') / W(\bar{\mathbf{x}})$ between different configurations are necessary. This makes the variational quantum Monte Carlo computationally feasible, as long as the weight W is known and easy to compute.

Within VMC, the expectation values appearing in the right-hand side of eq 20 or eq 21 are estimated statistically. In particular, in eq 20 the desired expectation value $\langle O \rangle$ is calculated as $(E(O)) / (E(D))$, being the nominator $E(O) = \langle O_L(\bar{\mathbf{x}}) \psi(\bar{\mathbf{x}})^2 / W(\bar{\mathbf{x}}) \rangle_{P(\bar{\mathbf{x}})}$ and the denominator $E(D) = \langle \psi(\bar{\mathbf{x}})^2 / W(\bar{\mathbf{x}}) \rangle_{P(\bar{\mathbf{x}})}$. Both the numerator and the denominator can be computed by generating a finite set of S independent points $\{\bar{\mathbf{x}}_s\}_{s=1,\dots,S}$ distributed according to the probability density distribution $P(\bar{\mathbf{x}})$ and typically generated with the Metropolis algorithm. Then, one can estimate $E(O)$ and $E(D)$ by standard averaging an appropriate function:

$$A_S[f, P] \equiv \frac{1}{S} \sum_{s=1}^S \frac{f(\bar{\mathbf{x}}_s) \psi(\bar{\mathbf{x}}_s)^2}{W(\bar{\mathbf{x}}_s)} \quad (22)$$

For a large but finite sampling S , the estimates $A_S[f, P]$ for the numerator and the denominator are affected by very correlated stochastic errors $\sigma_S[f, P]$, therefore special techniques are required to evaluate how this error affects the uncertainty in their ratio, whenever a nontrivial reweighting technique is employed. The standard deviation $\sigma_S[f, P]$ is defined as the square root of the variance of the estimate $A_S[f, P]$. If we assume the applicability of the central limit theorem, which in particular requires that the second moment of the probability distribution of $f(\bar{\mathbf{x}}_s) \psi(\bar{\mathbf{x}}_s)^2 / W(\bar{\mathbf{x}}_s)$ exists, we have that the probability distribution for the estimate $A_S[f, P]$ is normally distributed with mean $E[f]$ and standard deviation:

$$\sigma_S[f, P] \equiv \sqrt{\text{VAR}\{A_S[f, P]\}} = \sqrt{\frac{1}{S} \text{VAR}\left\{\frac{f(\bar{\mathbf{x}}_s) \psi(\bar{\mathbf{x}}_s)^2}{W(\bar{\mathbf{x}}_s)}\right\}} \quad (23)$$

For the sake of completeness, it should be mentioned that the applicability of the central limit theorem depends on some properties of the probability distribution of $f(\bar{\mathbf{x}}_s) \psi(\bar{\mathbf{x}}_s)^2 / W(\bar{\mathbf{x}}_s)$. The fact that the second moment exists only ensures the applicability of the theorem in its most general form, where the normality of the distribution is reached in the limit of infinite sampling $S \rightarrow \infty$. For a finite sampling $S < \infty$ the normal distribution is not generally satisfied, as it was indeed observed by J. R. Trail⁸² in the form of heavy tails.

Observe in eq 23 that the margin of uncertainty for the estimate of $E[f]$ using $A_S[f]$ goes to zero in the limit of infinite sampling $S \rightarrow \infty$. Moreover, if $\text{VAR}\{f(\bar{\mathbf{x}}_s) \psi(\bar{\mathbf{x}}_s)^2 / W(\bar{\mathbf{x}}_s)\}$ is finite, we have that the uncertainty $\sigma_S[f, P]$ on $A_S[f]$ converges to zero as $1/\sqrt{S}$, which is a very favorable scaling considering that there is no dependence on the dimensionality of the space ($3N$) where the sample points $\{\bar{\mathbf{x}}_s\}$ are defined.

Equation 23 also sheds lights on the importance of the probability density function P . A bad choice of W leads to a variance $\text{VAR}\{f(\bar{\mathbf{x}}_s) \psi(\bar{\mathbf{x}}_s)^2 / W(\bar{\mathbf{x}}_s)\}$ that is not even finite, whereas a good W yields a finite value of $\text{VAR}\{f(\bar{\mathbf{x}}_s) \psi(\bar{\mathbf{x}}_s)^2 / W(\bar{\mathbf{x}}_s)\}$, as we will see in the following sections. Moreover, whenever the estimator $O_L(\bar{\mathbf{x}}) = \bar{O}$ is independent of $\bar{\mathbf{x}}$ we see an important property in the calculation of physical expectation values, namely that, for any choice of the weight W , the evaluation of the ratio:

$$\langle O \rangle \equiv \frac{\sum_{s=1}^S \frac{O_L(\bar{\mathbf{x}}_s) \psi(\bar{\mathbf{x}}_s)^2}{W(\bar{\mathbf{x}}_s)}}{\sum_{s=1}^S \frac{\psi(\bar{\mathbf{x}}_s)^2}{W(\bar{\mathbf{x}}_s)}} \quad (24)$$

yields always the same value \bar{O} , namely has zero variance, regardless of the fact that both the numerator and the denominator may have finite variances. This highlights once more the fact that a method like bootstrap or jackknife^{83,84} is necessary to exploit the correlation between the numerator and the denominator in the evaluation of the standard deviation corresponding to the physical average $\langle O \rangle$.

In order to simplify the notation, in the following sections the functional dependence of the wave function ψ , the local operator O_L and the density probability distributions P and Π on $\bar{\mathbf{x}}$, will be left implicit.

3.2. Energy Evaluation. The most important quantity that is evaluated in VMC is the energy. Considering eqs 20 and 21, the energy evaluation is determined by the values of the *local energy* $H_L(\bar{\mathbf{r}}) \equiv (\psi^{-1} \hat{H} \psi)_{\bar{\mathbf{r}}}$ being \hat{H} the Hamiltonian operator. For instance, using the standard sampling technique, eq 21, the VMC evaluation of the energy $\mathcal{E}[\psi]$ for the wave function ψ , involves the calculation of

$$\mathcal{E}[\psi] = \frac{\int H_L(\bar{\mathbf{r}}) \psi^2 d\bar{\mathbf{r}}}{\int \psi^2 d\bar{\mathbf{r}}} \quad (25)$$

where the integration is over the $3N$ Cartesian coordinates $\bar{\mathbf{r}}$ of the electrons.

If we consider a wave function ψ_i , which is an eigenfunction of the Hamiltonian with eigenvalue E_i , the corresponding local energy is $H_L[\psi_i] = E_i$ independently of the point $\bar{\mathbf{x}}$, where it is evaluated. This is true in particular for the ground state (GS) of the system, that is typically the target of electronic structure calculations. This shows that, in case we are using an exact eigenfunction of the system and the standard sampling, the zero-variance principle is satisfied. Moreover, it can be seen that also by sampling with a general weight W , as in eq 20, an exact eigenfunction always fulfills the zero-variance principle.

However, in proximity of the *nodal surface* the local energy H_L is divergent, unless we are sampling an exact eigenfunction of the Hamiltonian. Indeed, if an electron in the system is close, say at a distance $\delta \ll 1$, to the nodal surface, we have that the wave function ψ vanishes linearly with this distance, that is, $\psi \propto \delta$, but for a generic ψ that is not an exact eigenfunction of \hat{H} , we have that $H\psi \propto 1$; therefore, the local energy diverges as $H_L \propto \delta^{-1}$. The application of the standard sampling, eq 21, leads to the integral $\int H_L \psi^2 d\bar{\mathbf{r}}$, which in the proximity of this divergence is $\propto \int_0^1 \delta^{-1} d\delta$;

therefore, it is well behaved. In order to have a stochastic error on $\langle \mathcal{H} \rangle$ that converges to zero as $1/\sqrt{S}$, it is also necessary that the variance is well behaved. The calculation of the variance for the standard sampling leads to the integral $\int H_L^2 \psi^2 d\mathbf{r}$, which in the proximity of the nodal surface is $\propto \int_0^1 1 d\delta$; therefore, the variance of the energy is also finite.

However, the standard sampling approach is problematic for the estimation of the nuclear forces, as it will be shown in Section 3.4, because its variance is not finite due to the divergences in proximity of the nodal surface. In order to overcome this problem, we have sampled both the energies and the forces using eq 20, with a density probability distribution P that is proportional to ψ^2 everywhere except in proximity of the nodal surface, where its value is a nonzero constant. The details of this sampling function P will be given in Section 3.5, and the method is called *reweighting sampling*. By using the reweighting sampling a stochastic evaluation of the nuclear forces as well as of the energy remains well behaved.

It is worth mentioning that other divergences can exist in the local energy, besides the one in proximity of the nodal surface, namely in the following cases: (i) the electron–nucleus coalescence, (ii) the electron–electron coalescence, and for open systems also (iii) for electrons approaching infinity. However, for the wave function we have considered in this work, the first two cases are already managed by the Jastrow factor, through the terms in eq 18 and eq 17 that satisfy respectively the nuclear–electron and the electron–electron cusp conditions. The divergence (iii) will be discussed in Section 3.5.

3.3. Wave Function Optimization. According to the variational principle, the exact ground state energy E_{GS} represents the lowest bound for any variational wave function, including the parametrized wave functions that are considered in VMC calculations. The set of parameters $\bar{\alpha}$ of the variational wave function are therefore optimized in order to minimize the corresponding variational energy $\mathcal{E}[\psi_{\bar{\alpha}}]$. As a consequence of the fact that the wave function is approaching to an eigenstate, also the variance of the energy decreases and approaches zero.

In order to optimize the variational parameters $\bar{\alpha}$, we use in this work the stochastic reconfiguration^{33,52} method (SR) and the more recent linear method^{61,85,86} based on an efficient estimate of the Hessian matrix (SRH). Both SR and SRH (for the details we refer to the cited references) are iterative methods where the variational parameters are evolved by incremental changes $\bar{\alpha} \rightarrow \bar{\alpha}' = \bar{\alpha} + \Delta\bar{\alpha}$ using the generalized force $\bar{f} \equiv -\partial\mathcal{E}[\psi_{\bar{\alpha}}]/\partial\bar{\alpha}$ acting on the parameters, and the matrix S , whose elements are $S_{kl} \equiv \langle (\partial/\partial\alpha_k)(\psi_{\bar{\alpha}}/\|\psi_{\bar{\alpha}}\|) | (\partial/\partial\alpha_l)(\psi_{\bar{\alpha}}/\|\psi_{\bar{\alpha}}\|) \rangle$, that takes into account the correlation between the parameters in the wave function. In SRH also partial information of the energy second derivatives is taken into account, and the method is generally faster and more efficient.

In particular, within SR, a generic parameter α_k is changed at each iteration by $\Delta\alpha_k = \Delta t \Sigma_k^{-1} f_k$, being Δt an appropriate small number. In case S is the identity matrix, the SR optimization would correspond to a simple *steepest descent* optimization of the wave function. The computational advantage of SR over a simple steepest descent, in terms of velocity of convergence, has been observed in several cases,⁸⁷ and it is roughly proportional to the condition number of the matrix S . Since in a correlated wave function the nonlinear coupling between different variational parameters makes this matrix necessarily very ill conditioned (with high condition number), the gain in the optimization may be often drastic, that is certainly true for large number of variational parameters. A recent work⁸⁸ provides a simple

geometrical interpretation of the advantage of the SR optimization over the steepest descent. Indeed, Mazzola et al.⁸⁸ have shown that the matrix S is actually the *metric*, to be intended in a differential geometry sense, where the parametrized normalized wave function $(\psi_{\bar{\alpha}})/(\|\psi_{\bar{\alpha}}\|)$ lives. According to this point of view, it follows that SR can be interpreted as a steepest descent in this curved space, where the parameters are moved in the direction of the force along locally orthogonal and independent directions.

3.4. Force Evaluation. If we assume the Born–Oppenheimer approximation and a classical description of the nuclei, the 3-dimensional force acting on atom a is, by definition:

$$\mathbf{F}_a \equiv -\nabla_a \mathcal{E}[\psi] \quad (26)$$

where $\nabla_a \equiv d/(d\mathbf{R}_a)$ is the gradient relative to the Cartesian coordinates \mathbf{R}_a of the nucleus a , and $\mathcal{E}[\psi]$ is the variational energy, as written in eq 25, associated to the electronic wave function ψ for a configuration $\bar{\mathbf{R}}$ of the atoms. The terms in $\mathcal{E}[\psi]$ that are functionally dependent on the atomic coordinates are the Hamiltonian $\hat{H} \equiv \hat{H}_{\bar{\mathbf{R}}}$ and the wave function $\psi \equiv \psi_{\bar{\alpha}, \bar{\mathbf{R}}}$, which has an implicit dependence on $\bar{\mathbf{R}}$ in the p parameters $\bar{\alpha} = \{\alpha_1, \dots, \alpha_p\} \equiv \bar{\alpha}_{\bar{\mathbf{R}}}$, which have to be optimized for each $\bar{\mathbf{R}}$ in order to minimize the variational energy, and also an explicit dependence, if ψ is defined using a local basis set, as in our work. Therefore the local energy $H_L \equiv (\hat{H}_{\bar{\mathbf{R}}} \psi_{\bar{\alpha}, \bar{\mathbf{R}}})/\psi_{\bar{\alpha}, \bar{\mathbf{R}}}$ that appears in $\mathcal{E}[\psi]$ depends on $\bar{\mathbf{R}}$ both through the wave function and the Hamiltonian.

By substitution of eq 25 into eq 26, it is straightforward to obtain the following *analytical* expression for the force:

$$\mathbf{F}_a = \mathbf{F}_a^{\text{HF}} + \mathbf{F}_a^{\text{P}} + \mathbf{F}_a^{\bar{\alpha}} \quad (27)$$

$$\begin{aligned} \mathbf{F}_a^{\text{HF}} &= -\frac{\int \frac{\partial H_L}{\partial \mathbf{R}_a} \psi^2 d\mathbf{r}}{\int \psi^2 d\mathbf{r}} \\ \mathbf{F}_a^{\text{P}} &= -2 \frac{\int (H_L - \mathcal{E}[\psi]) \frac{\partial \log |\psi|}{\partial \mathbf{R}_a} \psi^2 d\mathbf{r}}{\int \psi^2 d\mathbf{r}} \\ \mathbf{F}_a^{\bar{\alpha}} &= -\sum_{k=1}^p \frac{\partial \mathcal{E}[\psi]}{\partial \alpha_k} \frac{\partial \alpha_k}{\partial \mathbf{R}_a} \end{aligned}$$

where the three terms that constitute the total force: \mathbf{F}_a^{HF} , \mathbf{F}_a^{P} , and $\mathbf{F}_a^{\bar{\alpha}}$ are respectively given by the explicit dependence on \mathbf{R}_a of the local energy and of the wave function, and the implicit dependence on \mathbf{R}_a of the parameters of the wave function.

The term $\mathbf{F}_a^{\bar{\alpha}}$ is, in principle, the most complicated to be evaluated, because of this implicit dependence which makes the derivative $\partial\alpha_k/\partial\mathbf{R}_a$ difficult to evaluate. Fortunately, if the values of $\bar{\alpha}_{\bar{\mathbf{R}}}$ correspond to a minimum for the energy $\mathcal{E}[\psi]$, then $(\partial\mathcal{E}[\psi])/(\partial\alpha_k) = 0$ for the Euler condition, and $\mathbf{F}_a^{\bar{\alpha}} = 0$. For this reason the term $\mathbf{F}_a^{\bar{\alpha}}$ has been neglected in our calculations.

The other two terms, \mathbf{F}_a^{HF} and \mathbf{F}_a^{P} , are usually referred to as the Hellmann–Feynman term and the Pulay term, respectively. Actually the Hellmann–Feynman term \mathbf{F}_a^{HF} resembles the term $\int (\nabla_a \hat{H}) \Psi^2 d\mathbf{r}$ that comes from the application of the Hellmann–Feynman theorem, although it is not exactly the same because in general $\nabla_a H_L \neq \nabla_a \hat{H}$. Moreover, in VMC calculations, the Hellmann–Feynman theorem is not even applicable, because ψ is neither normalized nor an eigenstate of \hat{H} . But in the limit case where ψ is an eigenstate of \hat{H} , and consequently $H_L = E[\psi]$, the Pulay term \mathbf{F}_a^{P} is zero and the only contribution to the force comes from \mathbf{F}_a^{HF} . As a consequence of

this, it is expected that the more ψ approaches an eigenstate of \hat{H} , the lower is the \mathbf{F}_a^P component of the force.

The analytical expression of the force in eq 27 is correct and is significantly more accurate and efficient than the corresponding expression based only on the Hellmann–Feynman contribution, as observed by Sorella and Capriotti.⁴⁵ The efficiency is defined as the inverse of the computational time to reach the required stochastic precision, and in the specific case of the water dimer studied in ref 45, an improvement of 2 orders of magnitude was obtained. However, Sorella and Capriotti showed that a further improvement of about 1 order of magnitude is possible using the analytical expression with the differential *space warp coordinate transformation* (SWCT). Therefore, in this work we have used these SWCT analytical forces, that are obtained as follows.

SWCT was originally introduced by Umrigar⁴¹ for an efficient calculation of the forces but using only finite-difference derivatives. Within SWCT, a displaced \mathbf{D}_a of the nucleus a is followed by a displacement of the electrons. Each electron i is translated, in the direction \mathbf{D}_a , of a quantity that depends on its distance $r_{ia} = \|\mathbf{r}_i - \mathbf{R}_a\|$ with the nucleus a . If $r_{ia} \sim 0$ the displacement of electron i is $\sim \mathbf{D}_a$; if $r_{ia} \rightarrow \infty$ the displacement is ~ 0 . In this way, the electronic coordinates $\bar{\mathbf{r}}$ mimic the displacement of the charge around the nucleus \mathbf{R}_a . More in detail, following refs 45 and 80, SWCT is described by the following transformation of the nuclear and electronic coordinates:

$$\mathbf{R}_b \rightarrow \mathbf{R}'_b = \mathbf{R}_b + \mathbf{D}_a \quad (28)$$

$$\mathbf{r}_i \rightarrow \mathbf{r}'_i = \mathbf{r}_i + \omega(r_{ia})\mathbf{D}_a$$

for $b = 1, \dots, M$ and $i = 1, \dots, N$. In the above equation the weight that quantifies the amount of electronic displacement is chosen to be:

$$\omega(r_{ia}) = \frac{r_{ia}^{-4}}{\sum_{b=1}^M r_{ib}^{-4}} \quad (29)$$

according to refs 40, 45, and 80.

The variational energy $\mathcal{E}_{\bar{\mathbf{R}}'}[\psi_{\bar{\alpha}, \bar{\mathbf{R}}}]$ calculated in the nuclear coordinates $\bar{\mathbf{R}}'$, for an infinitesimal displacement \mathbf{D}_a , considering also that the displacement of the parameters $\Delta\bar{\alpha} = \bar{\alpha}_{\bar{\mathbf{R}}'} - \bar{\alpha}_{\bar{\mathbf{R}}}$ is negligible at the first order as discussed previously, is given by

$$\mathcal{E}_{\bar{\mathbf{R}}'}[\psi_{\bar{\alpha}, \bar{\mathbf{R}}}] = \frac{\int H_L^{\bar{\mathbf{R}}'}[\psi_{\bar{\alpha}, \bar{\mathbf{R}}}(\bar{\mathbf{r}}')] \psi_{\bar{\alpha}, \bar{\mathbf{R}}}(\bar{\mathbf{r}}')^2 d\bar{\mathbf{r}}'}{\int \psi_{\bar{\alpha}, \bar{\mathbf{R}}}(\bar{\mathbf{r}}')^2 d\bar{\mathbf{r}}'} \quad (30)$$

where the integrated electronic coordinates $\bar{\mathbf{r}}$ can be substituted by the SWCT expression in eq 28, and $d\bar{\mathbf{r}}' = \det(\partial\bar{\mathbf{r}}'/\partial\bar{\mathbf{r}}) d\bar{\mathbf{r}}$. We obtain in this way an expression that we call $E_{\bar{\mathbf{R}}'}^{\text{SWCT}}$.

The SWCT analytic force $\mathbf{F}_a^{\text{SWCT}}$ is then obtained by differentiating the energy $E_{\bar{\mathbf{R}}'}^{\text{SWCT}}$ over \mathbf{D}_a and evaluating it at $\mathbf{D}_a = 0$:

$$\mathbf{F}_a^{\text{SWCT}} = - \left. \frac{d\mathcal{E}_{\bar{\mathbf{R}}'}^{\text{SWCT}}}{d\mathbf{D}_a} \right|_{\mathbf{D}_a=0} \quad (31)$$

It has to be noted that, in this case, we have also an implicit dependence of the electronic coordinates on \mathbf{D}_a yielding additional force terms arising from the derivative of the wave function over the electrons coordinates, $\partial\psi/\partial\mathbf{r}_i$, and to the derivative of the Jacobian of the SWCT. The calculation in eq 31 leads straightforwardly to an expression for the force analogous to eq 27 where the Hellmann–Feynman and the Pulay terms can be easily identified:

$$\mathbf{F}_a^{\text{SWCT}} = \mathbf{F}_a^{\text{SWCT-HF}} + \mathbf{F}_a^{\text{SWCT-P}} \quad (32)$$

$$\mathbf{F}_a^{\text{SWCT-HF}} = - \frac{\int (\nabla_a^{\text{SWCT}} H_L) \psi^2 d\bar{\mathbf{r}}}{\int \psi^2 d\bar{\mathbf{r}}}$$

$$\mathbf{F}_a^{\text{SWCT-P}} = -2 \frac{\int (H_L - E[\psi]) (\nabla_a^{\text{SWCT}} \log|\psi|) \psi^2 d\bar{\mathbf{r}}}{\int \psi^2 d\bar{\mathbf{r}}}$$

Indeed, the above expression is almost identical to eq 27 with the difference that we have introduced here a generalized gradient ∇_a^{SWCT} , defined in the following way:

$$\nabla_a^{\text{SWCT}} H_L \equiv \frac{\partial H_L}{\partial \mathbf{R}_a} + \sum_{i=1}^N \omega(r_{ia}) \frac{\partial H_L}{\partial \mathbf{r}_i} \quad (33)$$

$$\nabla_a^{\text{SWCT}} \log|\psi| \equiv \frac{\partial \log|\psi|}{\partial \mathbf{R}_a} + \sum_{i=1}^N \left(\omega(r_{ia}) \frac{\partial \log|\psi|}{\partial \mathbf{r}_i} + \frac{1}{2} \frac{\partial \omega(r_{ia})}{\partial \mathbf{r}_i} \right)$$

for the Hellmann–Feynman and the Pulay terms, respectively.

As discussed exhaustively by Sorella Capriotti,⁴⁵ the implementation of the computational technique of the *adjoint algorithmic differentiation* (AAD) allows a computationally very efficient evaluation of all the terms appearing in eq 31, that roughly can be evaluated in $\propto N^3$ operations. This technique leads to a computational cost for the evaluation of the energy and all the force components amounting to about four times the time required for the calculation of the variational energy alone. The computational gain is substantial, especially if compared with finite difference methods on large systems.^{24,45}

At this point, we have the exact expressions for the analytical forces and the technical instruments to calculate all the components efficiently. However, there is still a point that has to be addressed: do these expressions lead to quantities that can be efficiently evaluated within a stochastic approach, for a wave function ψ that in general only approximates the exact GS solution? As discussed in Section 3.1, this implies that we have to choose the appropriate weight W allowing the stochastic evaluation of the expectation value of the force; that is, the variance in eq 23 has to be finite.

Let us start considering the terms containing divergences, which could lead to an infinite variance, starting from the Hellmann–Feynman force. We can easily recognize the two problematic terms $\partial H_L / \partial \mathbf{R}_a$ and $\partial H_L / \partial \mathbf{r}_i$, respectively in the cases of electron–nucleus and of electron–electron coalescence. Indeed the derivatives of the potential energy ∂V , included in ∂H_L , contains terms which would give an infinite variance, namely $\partial V / \partial \mathbf{r} \propto \delta_{ee}^{-2}$ for the electron–electron distance $\delta_{ee} \ll 1$ and $\partial V / \partial \mathbf{R} \propto \delta_{en}^{-2}$ for the electron–nucleus distance $\delta_{en} \ll 1$. However, in our case, we can handle these divergences because we are using wave functions that satisfy the cusp conditions, producing a divergence in the kinetic term of the same amount but of opposite sign with respect to the divergence of the potential, regularizing in this way the divergence of H_L and of its derivatives.

Nevertheless, $\partial H_L / \partial \mathbf{R}_a$ and $\partial H_L / \partial \mathbf{r}_i$ remain divergent in proximity of the nodal surface. We have already mentioned in Section 3.2 that in general $\psi \propto \delta$ and $H_L \propto \delta^{-1}$ at a distance $\delta \ll 1$ from the nodal surface, hence $\partial H_L \propto \delta^{-2}$. Using the standard

sampling technique these divergences would lead to a variance that in proximity of the nodal surface is $\propto \int_0^1 \delta^{-2} d\delta$, therefore unbounded. However, with the *reweighting sampling* method described in Section 3.5, the variance becomes $\propto \int_0^1 \delta^0 d\delta$; thus, its divergence is completely under control and the variance is finite.

Also, in the Pulay force there is a similar problematic behavior in proximity of the nodal surface, because both H_L and $\partial \log |\psi|$ diverge as δ^{-1} , giving an infinite variance if the standard sampling is used. The use of the reweighting sampling regularizes also this term, giving a finite variance.

3.5. Reweighting Method for Open Systems. Attaccalite and Sorella proposed a reweighting method to solve the infinite variance issue in the proximity of the nodal surface by using a different probability distribution $P(\bar{\mathbf{x}}) \propto W(\bar{\mathbf{x}}) = \psi_G(\bar{\mathbf{x}})^2$, defined in terms of a *guiding function* $\psi_G(\bar{\mathbf{x}})$, rather than the standard sampling $\Pi(\bar{\mathbf{x}}) \propto \psi(\bar{\mathbf{x}})^2$.

The guiding function $\psi_G(\bar{\mathbf{x}})$ is defined in terms of the wave function $\psi(\bar{\mathbf{x}})$ as follows:

$$\psi_G(\bar{\mathbf{x}}) = \frac{R^e(\bar{\mathbf{x}})}{R(\bar{\mathbf{x}})} \psi(\bar{\mathbf{x}}) \quad (34)$$

where $R(\bar{\mathbf{x}})$ is proportional to the distance δ from the nodal surface, for $\delta \ll 1$, and vanishes in the same way $\psi(\bar{\mathbf{x}})$ does, namely $\psi(\bar{\mathbf{x}}) \propto R(\bar{\mathbf{x}})$. The $R^e(\bar{\mathbf{x}})$ is the function that regularizes ψ_G in the vicinity of the nodal surface, namely for $\delta \propto R(\bar{\mathbf{x}}) < \varepsilon$, and it is defined as

$$R^e(\bar{\mathbf{x}}) = \begin{cases} R(\bar{\mathbf{x}}) & \text{if } R(\bar{\mathbf{x}}) \geq \varepsilon \\ \varepsilon [R(\bar{\mathbf{x}})/\varepsilon]^{R(x)/\varepsilon} & \text{if } R(\bar{\mathbf{x}}) < \varepsilon \end{cases} \quad (35)$$

where the nontrivial regularization for $R(\bar{\mathbf{x}}) < \varepsilon$ is introduced in order to satisfy the continuity of the first derivative of $\psi_G(\bar{\mathbf{x}})$. The guiding function $\psi_G(\bar{\mathbf{x}})$ defined in this way and its corresponding probability density function $P(\bar{\mathbf{x}}) \propto \psi_G(\bar{\mathbf{x}})^2$ define a *reweighting factor*

$$\left(\frac{\psi(\bar{\mathbf{x}})}{\psi_G(\bar{\mathbf{x}})} \right)^2 = \left(\frac{R(\bar{\mathbf{x}})}{R^e(\bar{\mathbf{x}})} \right)^2 = \min \left[1, \left(\frac{R(\bar{\mathbf{x}})}{\varepsilon} \right)^{2(1-\frac{R(\bar{\mathbf{x}})}{\varepsilon})} \right] \quad (36)$$

that vanishes in the proximity of the nodal surface, namely $R(\bar{\mathbf{x}}) \propto \delta^2$, whereas the probability density function $P(\bar{\mathbf{x}}) \propto \varepsilon^2 (\psi(\bar{\mathbf{x}})/R(\bar{\mathbf{x}}))^2 \propto \varepsilon^2$ remains constant but finite. This $P(\bar{\mathbf{x}})$ slightly enhances the sampling in the vicinity of the nodal surface where $\Pi(\bar{\mathbf{x}})$ vanishes. So far, our reweighting method removes the singularities up to δ^{-2} and provides finite variance.

The regularization scheme which Attaccalite and Sorella⁴⁴ proposed to evaluate $R(x)$ is based on the matrix \mathbf{A} that appears in the determinantal (antisymmetric) part of the QMC wave function, eq 1. For the AGP wave functions used in this work, we can identify the matrix \mathbf{A} with the \mathbf{M}^{AGP} described in Section 2.2. As soon as the configuration of electrons approaches the nodal surface, $\det(\mathbf{A}) \rightarrow 0$ and the elements of the \mathbf{A}^{-1} grow extremely large. According to this feature, the regularizing is chosen to be controlled by \mathbf{A}^{-1}_{ij} in the following way:

$$R(\bar{\mathbf{x}}) = \left(\sum_{i,j} |\mathbf{A}_{ij}^{-1}|^2 \right)^{-1/2} \quad (37)$$

However, within this scheme eq 37 does not take into account the case of open systems such as isolated atoms and molecules (type 4 in ref 82). As an electron i samples a region very far from

the center of mass r_0 of the nuclei, namely $r_{i0} = \|\mathbf{r}_i - \mathbf{r}_0\| \gg 1$, the decay of the many-body wave function is dominated by the determinantal part as the Jastrow correlation is identically one in this limit. A simple inspection shows that $\det(\mathbf{A})$ behaves as $\propto \exp(-\tilde{z}_{\min} r_{i0})$ [$\propto \exp(-\tilde{z}_{\min}^2 r_{i0}^2)$], where \tilde{z}_{\min} is the minimum exponent in the Slater [Gaussian] basis. The old regularization in eq 37 vanishes clearly in the same way. To verify this behavior it is enough to apply the Rouché–Capelli theorem stating that the inverse matrix elements A_{ij}^{-1} can be expressed with the ratio of a cofactor matrix determinant ($\det C_{ji}$) and the determinant itself, namely:

$$A_{ij}^{-1} = \frac{\det C_{ji}}{\det(\mathbf{A})}$$

Now, we immediately arrive to the bad conclusion that the probability distribution $P(\bar{\mathbf{x}})$ is ill defined as it converges to a constant in the limit when $r_{i0} \gg 1$, because, $R(\bar{\mathbf{x}}) \rightarrow 0$ in the same way as $\psi(\bar{\mathbf{x}}) \rightarrow 0$ (as discussed above), and the resulting distribution $P(\bar{\mathbf{x}})$ is not normalizable. In practice, this means that the random walk for long enough simulation will be unstable, and all electrons are pushed to very large distance from the atoms, providing unpredictable and certainly biased results.

In order to overcome this clear instability, we replace the \mathbf{A} in eq 37 with \mathbf{A}' . The new matrix \mathbf{A}' is defined by changing its asymptotic behavior for large r_{i0} :

$$A'_{ij} = A_{ij} \exp(zr_{i0} + zr_{j0}) \quad (38)$$

where z can be any positive value. In fact, the new regularization will act in the same way close to the nodes of ψ , whereas when $r_{i0} \gg 1$, $\det(\mathbf{A}')$ decays as $\exp[-\tilde{z}_{\min}^2 r_{i0}^2 + zr_{i0}]$ for a Gaussian basis, and for a Slater basis, if $\tilde{z}_{\min} > z$, it decays as $\exp[-(\tilde{z}_{\min} - z)r_{i0}]$ and diverges otherwise. Therefore, $P(\bar{\mathbf{x}})$, by using this new definition of $R(\bar{\mathbf{x}})$, will decay as $\exp(-2zr_{i0})$ in the former cases, or as Ψ^2 itself in the latter case, yielding in any case a perfectly defined and normalizable distribution.

In practice, if z is too small, \mathbf{A}' behaves too much like \mathbf{A} and the instability remains. On the other hand, if z is too large, the probability distribution $P(\bar{\mathbf{x}})$, as we have seen, remains too close to the original one $\simeq \Psi^2$ for electron-ion distances $\gg 1/z$, and therefore in this region the singularities in the nodal surfaces remain, and the regularization is not effective also in this case. Therefore, with this simple trick, and a reasonable value of $z \simeq 1/\xi$, where ξ is the linear dimension of the important region of nonvanishing charge density, this numerical instability, present in open systems, is readily removed, and the singularities around the nodal surfaces are perfectly controlled, because the proposed regularization works exactly as the previous one⁴⁴ adopted for PBC. Indeed, if electrons are close to this nodal surface $\det(\mathbf{A}) = 0$ and r_{i0} are all finite, the following equality

$$\det(\mathbf{A}') = \prod_i^N \exp(zr_{i0}) \det(\mathbf{A}) \quad (39)$$

implies that the new regularization works as well as the previous one, being the factor $\prod_i^N \exp(zr_{i0})$ just an irrelevant term.

3.6. Charge Density and Dipole and Quadrupole Evaluation. Several important properties of the molecular systems, such as the dipole and the quadrupole, derive from the charge density distribution:

$$\rho(\mathbf{r}) \equiv \sum_a^M Z_a \delta(\mathbf{r} - \mathbf{R}_a) - \left\langle \sum_i^N \delta(\mathbf{r} - \mathbf{r}_i) \right\rangle_{\Pi} \quad (40)$$

where the first term in the right-hand side is due to the nuclear charges Z_a centered in their Cartesian coordinate \mathbf{R}_a , in agreement with the Born–Oppenheimer approximation and classical nuclei. The second element in the right-hand side, which is due to the electronic charges, is averaged over the distribution of the electrons $\Pi \propto \psi^2$.

From the definition in eq 40 of the charge density, it is straightforward to obtain the expression for the dipole \mathbf{D} :

$$\mathbf{D}^\alpha \equiv \int \mathbf{r}^\alpha \delta(\mathbf{r}) \, d\mathbf{r} \quad (41)$$

$$= \sum_a^M Z_a \mathbf{R}_a^\alpha - \left\langle \sum_i^N \mathbf{r}_i^\alpha \right\rangle_\Pi \quad (42)$$

and for the traceless quadrupole tensor:

$$Q^{\alpha\beta} \equiv \frac{1}{2} \int (3r_i^\alpha r_i^\beta - \|\mathbf{r}_i\|^2 \delta^{\alpha\beta}) \delta(\mathbf{r}) \, d\mathbf{r} \quad (43)$$

$$= \frac{1}{2} \sum_a^M Z_a (3\mathbf{R}_a^\alpha \mathbf{R}_a^\beta - \|\mathbf{R}_a\|^2 \delta^{\alpha\beta}) - \frac{1}{2} \left\langle \sum_i^N (3\mathbf{r}_i^\alpha \mathbf{r}_i^\beta - \|\mathbf{r}_i\|^2 \delta^{\alpha\beta}) \right\rangle_\Pi \quad (44)$$

where α and β label the three Cartesian axes and $\delta^{\alpha\beta}$ is the Kronecker's delta.

The dipole depends on the choice of the reference frame, unless the total charge of the molecule is zero, and the quadrupole depends on the choice of the reference frame, unless the dipole is zero. For the case of the water molecule, considered in this paper, the total charge is zero, but the dipole is not zero. Therefore, we have to define the reference frame, in order to compare with the experimental and other calculated values of the quadrupole.

The electronic part of the dipole and of the quadrupole have been calculated by averaging within a VMC scheme the quantities of interest. We are aware that more sophisticated improved estimators for the density and related quantities are available in literature;^{50,89} however, they are not necessary for this work.

3.7. Energy Evaluation by Fixed Node Projection Monte Carlo. Using the projection Monte Carlo approaches, it is possible to access the lowest possible energy, with the constraint that Φ has the same nodal surface of an appropriately chosen guiding function Ψ (fixed node approximation).^{4,5} Therefore, it is of fundamental importance to choose a guiding function with a reliable nodal surface, and for this purpose, it is usually considered the variational wave function with minimum possible energy within a given ansatz.

Among the different projection methods, we have considered in this work the lattice regularized diffusion Monte Carlo.^{13,14} LRDMC is based on the spatial discretization of the molecular Hamiltonian on a lattice of mesh size a , and it resorts to the projection scheme used also in the Green function Monte Carlo algorithm.^{11,12} This method has two very interesting properties: it maintains its efficiency even for systems with a large number of electrons;¹⁴ and it preserves the variational principle even when used in combination with nonlocal pseudopotentials.¹⁴ The error induced by the finite mesh size a is analogous to the time step error appearing in standard DMC calculations. It can be controlled by performing several calculations with different

values of the mesh a and finally extrapolating to the continuum limit $a \rightarrow 0$.

4. COMPUTATIONAL DETAILS

QMC Package. The QMC energy and force calculations have been carried out using the *TurboRVB* package developed by S. Sorella and co-workers,⁹⁰ which includes a complete suite of variational and diffusion quantum Monte Carlo calculations on molecules and solids and for wave function and geometry optimization.

Description of the Core Electrons. The results that are presented here have been obtained both by all electrons (AE) calculations, and by calculations where the two core electrons of the oxygen atom have been described using a pseudopotential. In order to appreciate the reliability of the calculations with the pseudopotential versus the AE calculations, two different pseudopotentials have been used and compared in this work: the scalar-relativistic energy consistent pseudopotential (ECP) of Burkatzki et al.⁹¹ and the smooth relativistic norm-conserving pseudopotential (NCP) of Trail and Needs.⁹²

Wave Function Ansatzes. In this work, we have considered several many-body wave functions, which have been constructed starting from the terms described in Section 2:

JAGP: a Jastrow correlated AGP wave function, with the Jastrow factor and the determinantal part described in Section 2.5 and in Section 2.2, respectively.

JSD: a Jastrow correlated single determinant wave function, with the Jastrow factor and the determinantal part described in Section 2.5 and in Section 2.3, respectively.

JAGPn*: a Jastrow correlated constrained AGPn* wave function, with the Jastrow factor and the determinantal part described in Section 2.5 and in Section 2.4, respectively.

JDFT: combination of the Jastrow factor described in Section 2.5 with a single determinant wave function, obtained by the Kohn–Sham orbitals of a DFT calculation within local-density approximation (LDA) as described in ref 93 and implemented in the *TurboRVB* package.⁹⁰ This wave function, also studied in ref 90 is actually a JSD, but it is called differently to highlight that in JDFT, at variance of JSD, the determinantal part has been optimized by a DFT calculation and only the parameters of the Jastrow term have been variationally optimized by QMC.

The Basis Set. As discussed in Sections 2.2–2.5, both the determinantal and the Jastrow part of the wave function use atomic orbitals (see description in Section 2.1). The number and the type of the atomic orbitals is a nontrivial choice for QMC calculations, as for other quantum chemical methods, because if the basis set is too small the results are biased. Anyway, in QMC, a large basis set introduces a large number of parameters that are computationally expensive to optimize, leading, in the worst cases, to instabilities in the optimization. In this work, the basis set convergence for the Jastrow and the determinantal terms is studied.

The determinantal term is functionally similar to the wave functions used in HF, DFT, or post-HF calculations; therefore, we constructed and used several basis that are inspired by some of the standard basis used in quantum chemistry and, in particular, the Dunning's basis.^{94,95} However, the peculiarities of the QMC wave functions, namely the presence of the Jastrow term and the use of particularly smooth pseudopotentials, allows a large reduction of the size of the basis set and, as a consequence, the number of parameters required for the optimization of the energy. For instance, the largest exponents (suitable to correctly describe the core) can be eliminated, because they are already described with a reasonable accuracy by the electron–nucleus

interaction term in the Jastrow, satisfying exactly the electron-nucleus cusp condition. Conversely, the most diffusive Gaussian exponents can be safely replaced by very few but tunable STO orbitals (one for each angular momentum) introduced in the atomic basis of the determinantal part. The list of the basis sets considered in this work for the determinantal part, with the source basis, the filter criteria, and the number of parameters introduced by each basis are reported in Table S1 of the Supporting Information. Most of the orbitals are GTO, as the source basis are GTO, but in some cases, an extra STO orbital was introduced, in order to better describe the diffusion part of the orbital and to have the theoretical long-range exponential decay of the wave function. Clearly, the filter is slightly different if the pseudopotential is or is not used. The basis set convergence for the determinantal part is discussed in Section 5.2.

The choice of the basis set for the Jastrow term is more challenging, because this term is a peculiar feature of the QMC calculations, and we do not have a preoptimized or precharacterized basis coming from other methods. Moreover, the choice of a large enough basis set for the Jastrow is very important for the JAGP and JAGPn* ansatzes, not only for the improvement in the dynamical correlation of the wave function but also because only in the limit of a complete Jastrow factor the unphysical charge fluctuations of the AGP are suppressed and the wave function becomes size consistent, as discussed by Sorella et al.³³ and recently by Neuscamman.⁶³ In this work, we only tested several GTO atomic orbitals for the Jastrow, both uncontracted, contracted, and with hybrid contraction. The performances of the different choices are discussed in Section 5.1.

Wave Function Parameters. The different wave function ansatzes used in this work depends on several parameters, which have to be optimized variationally as explained in Section 3.3. Four main classes of such parameters can be identified:

1. the coefficients and the exponents appearing both in the determinantal basis set $\{\phi_{\mu_a}^a\}$ and in the Jastrow basis set $\{\chi_{\mu_a}^a\}$
2. the elements of the Jastrow matrix $f_{v_a v_b}^{a,b}$ of the inhomogeneous electron–electron term in eq 19
3. the Jastrow parameters b_1 and b_2 of the homogeneous one-electron and two-electrons interaction terms, respectively, in eq 18 and in eq 17
4. for the JAGP ansatz: the elements of the Λ matrix, see eq 9; or for the JSD and the JAGPn* ansatz: the leading eigenvectors and eigenvalues of Λ , that is, the MOs and their weights, see eq 11

As already mentioned, for a JDFT ansatz only the Jastrow terms have to be variationally optimized, because the determinantal part is directly obtained by a DFT-LDA calculation. However, the remaining ansatzes, namely the JSD, JAGPn*, and JAGP, differ by the number and kind of parameters to be optimized; thus, also the optimization schemes are different. The optimization protocols are described in the Supporting Information, Section 1.

It has to be observed that the exponents appearing in the determinantal part are already preoptimized by other computational approaches, although their values are not the optimal ones for a QMC calculation, as they can be further improved by minimizing the variational energy. Their optimization is often quite challenging due to the nonlinear way they determine the wave function. Consequently, they have to be optimized using a large statistics, and by moving slowly and carefully during the

optimization. If they are not optimized, the energy minimization is more stable and easier, and this generally leads to a computational gain. For this reason, both the cases are considered in this work, and they are marked using the following labels:

Opt:noZ: the wave function optimization was carried on the determinantal matrix, the contraction coefficients in the determinantal basis set, and all the Jastrow terms, including the exponent values in the Jastrow basis

Opt:all: all the parameters are optimized, including the exponents in the determinantal part

Reference Structure. The reported single point calculations are referred to the experimental structure of the water molecule,⁶⁸ having the oxygen–hydrogen distance of $r_{\text{OH}} = 0.95721(3)\text{\AA}$ and the angle between hydrogen–oxygen–hydrogen of $\phi_{\text{HOH}} = 104.522(5)$ degrees. Moreover, we have chosen the reference frame of the center of the mass (this is relevant for the quadrupole calculation). The water molecule is in the *xy*-plane, with the bisector of the HOH angle along the *y*-axis, with the oxygen in the *y*-axis and with negative value, and the hydrogens with positive *y* values. Thus, for symmetry reasons the only non negative coordinate of the dipole is the one along the *y* axis, and it is positive because the oxygen is more electronegative than the hydrogens.

Evaluation of the Equilibrium Structure and the Frequencies. In Section 5.4, we will report the values of the nuclear configuration at the minimum of the potential energy surface (PES), of the harmonic vibrational frequencies and of the anharmonic corrections, relative to VMC calculations for several different wave function ansatzes. The accurate determination of this quantities, and in particular of the frequencies, is challenging for methods like QMC, that are affected by a stochastic error that is several orders of magnitudes larger than the numerical error present in nonstochastic methods. In order to control the propagation of the errors on the predicted quantities, it is important to adopt a method that takes explicitly into consideration the presence of the stochastic error. In a recent work,⁵¹ some of us have shown how this can be achieved, by performing several single point calculations of the energies and the forces in a grid centered around a good guess of the minimum of the PES. The values of the energies or the forces are then used to perform a multidimensional fit of the PES, to obtain a better estimate of the minimum and of the vibrational properties. The choice of the grid is very important in this approach, in order to have reasonably small stochastic errors of the frequencies, of the order of a few cm^{-1} . The results reported in Section 5.4 are obtained using a grid of 59 points, and the displacements between these points are $\Delta r = 0.08$ a.u. for the OH distance and $\Delta\phi = 10$ degrees for the HOH angle (corresponding to “mesh-4” in ref 51). The experimental configuration of the molecule was taken as the initial guess of the PES structural minimum, which has a residual force of the order of 10^{-3} a.u. Although the same wave function is used to describe each of the 59 point in the grid, the nuclear coordinates are changed and consequently the wave function parameters have to be optimized independently. This has been done in a computationally convenient way by taking as initial guess the already optimized wave function for the configuration at the center of the grid. Moreover, we have carefully checked for some points in the grid that this procedure does not introduce any bias, by comparing with a standard optimization “from scratch”.

5. RESULTS AND DISCUSSION

Irrespective of the ansatz (JDFT, JSD, JAGPn*, or JAGP), in a QMC wave function two distinct and adequately large basis sets have to be chosen, respectively for the determinantal part and for the Jastrow factor. Too small bases may introduce a bias on the results, but too large bases make the wave function difficult or impossible to optimize, due to the stochastic nature of the approach and because the parameters become highly correlated. In Section 5.1, we discuss the basis set convergence for the Jastrow factor, while in Section 5.2 we discuss the convergence for the determinantal part, in the different ansatzes. In Section 5.3, we discuss the ionization and the atomization energies, and finally, in 5.4, we consider the properties of the PES obtained with different QMC approaches.

5.1. Basis Set Convergence for the Jastrow Factor. Since the Jastrow factor is peculiar of the QMC wave functions, little help for the choice of the basis set for its inhomogeneous part comes from other computational methods. Therefore, we have tested several basis for the Jastrow factor, in a wave function whose determinantal part was kept fixed. The considered ansatz is a JAGP function, with ECP pseudopotential for the two core electrons of the oxygen atom, and with a basis for the AGP part that is $O(4s,4p,1d)/[2s,2p,1d]$, $H(4s,1p)/[2s,1p]$, where the initial guess for the values of the exponents was inspired from the Dunning's cc-pVDZ basis. Despite this basis is relatively small, it is able to provide reliable results, as shown for instance in Zen et al.⁵¹ for the equilibrium structure of the water molecule.

We have considered uncontracted, contracted, and hybrid atomic contracted basis, both with the optimization schemes *opt:noZ* and *opt:all*. The complete list of all the obtained values for the energy, the variance, the dipole, and the quadrupole are reported in the Supporting Information, in Tables S2 and S3. Looking at the values of energy and variance, it is quite evident that the uncontracted orbitals in the Jastrow provides much better results than the contracted or the hybrid atomic contracted orbitals. This is probably due to the fact that the 3-body term, see eq 19, gain a considerable variational advantage by the flexibility of an uncontracted basis. Thus, the choice of the optimal basis for the Jastrow factor should be an uncontracted basis. Focusing only on the latter, in Figure 1, we show the basis set convergence of the energy, the variance, the dipole and the Q^{xx} component of the quadrupole.

Several observations can be done. First, it is clear that the optimization of the exponents, *opt:all*, leads to a large improvement in the wave function, as reflected in all the properties considered. This improvement is particularly significant if the basis is rather small, whereas it is relatively small for a large basis. Second, it is interesting to note that the presence of the *d* orbitals in the oxygen basis of the Jastrow (highlighted with a gray background in the figure) highly improves the dipole and the quadrupole. Third, we can observe the expected correlation between the energy and the variance: a lower energy is connected to a lower variance (see also Figure S1(a) of the Supporting Information). A similar correlation is also expected with the charge distribution, and with the dipole in particular. A general improvement of the dipole is observed with the large basis sets, with low variances and low energies, but the convergence seems much more noisy than in the case of the energy (see Figure S1(b) of the Supporting Information). This is due to the fact that the dipole is not a function of the total energy; thus, the improvement in the variational energy, which is

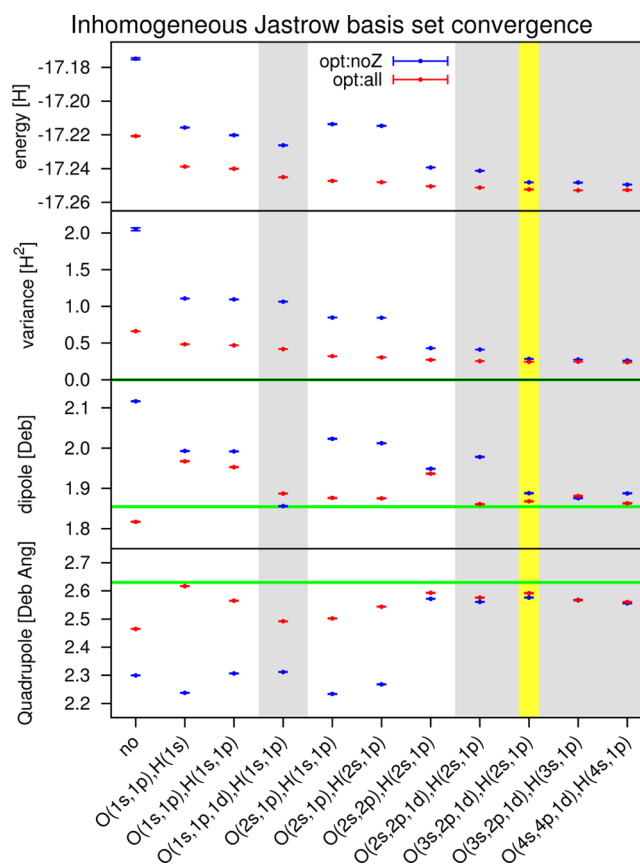


Figure 1. Basis set convergence of the water molecule VMC energy, variance, dipole, and Q^{xx} quadrupole for the Jastrow inhomogeneous term is shown here. The considered wave function is a JAGP, with ECP pseudopotential for the two core electrons of the oxygen, and $O(4s,4p,1d)/[2s,2p,1d]$, $H(4s,1p)/[2s,1p]$ determinantal basis. The Jastrow basis set is reported in the abscissa, and the basis with *d*-orbitals have been highlighted with a gray background. A yellow background has been used to indicate the basis considered for the following calculations. The results corresponding to *Opt:noZ* and *Opt:all* are reported in blue and red, respectively. In green, we report the expected exact value, corresponding to zero variance, and the experimental values of the dipole and quadrupole.

enforced during the wave function optimization, does not necessarily imply an improvement in the charge distribution.

The Jastrow basis that we have selected for the following calculations is $O(3s,2p,1d)$, $H(2s,1p)$, corresponding to the results highlighted in yellow in Figure 1. It represents an optimal balance between the accuracy of the results and the number of variational parameters, so the computational cost and the stability of the optimization.

5.2. Basis Set Convergence for the Determinantal Part and the Wave Function Ansatzes. Having defined the basis set for the Jastrow factor, we investigate now the different wave function ansatzes, namely JDFT, JSD, JAGPn*, and JAGP, with different description of the core electrons of the oxygen: using the ECP⁹¹ or NCP⁹² pseudopotentials, or all electron calculations. As for the Jastrow factor, also here, we have explored several basis sets for each wave function type, studying the basis set convergence. The complete list of the attempted combinations is reported in the Supporting Information, where in Tables S4 we show the convergence of the energy and the variance and in Tables S5 and S6, we consider also the dipole and the quadrupole. Some interesting aspects can be observed from

Table 1. VMC Evaluation of the Energy [H], the Variance [H^2], the Dipole [Deb], and the Diagonal Elements Q^{xx} , Q^{yy} , Q^{zz} of the Traceless Quadrupole Tensor [Deb·Å] for the Water Molecule, Compared with Other Accurate *Ab Initio* Evaluations and Experimental Results^a

function/core/basis ^b	no. param. ^c	energy	variance	dipole	Q^{xx}	Q^{yy}	Q^{zz}
JDFT/ECP/hybrid	(33) + 724 + 210	−17.24548(8)	0.3606(3)	1.9059(8)	2.5796(9)	−0.1551(9)	−2.4245(9)
JSD/ECP/uncontracted	14 + 0 + 666	−17.24820(5)	0.2734(2)	1.8881(4)	2.5842(5)	−0.1711(5)	−2.4131(5)
JSD/ECP/contracted	40 + 10 + 14878	−17.2482(1)	0.2668(10)	1.8755(10)	2.596(1)	−0.155(1)	−2.441(1)
JSD/ECP/hybrid	33 + 1086 + 465	−17.24824(7)	0.2692(1)	1.8877(6)	2.5819(7)	−0.1445(7)	−2.4374(6)
JAGPn*/ECP/contracted	40 + 10 + 14878	−17.2513(1)	0.2489(7)	1.8629(10)	2.570(1)	−0.149(1)	−2.421(1)
JAGP/ECP/uncontracted	14 + 0 + 666	−17.2536(2)	0.239(1)	1.8881(10)	2.579(1)	−0.174(1)	−2.406(1)
JAGP/ECP/contracted	(26) + 4 + 4186	−17.2529(1)	0.2665(7)	1.8609(10)	2.580(1)	−0.147(1)	−2.433(1)
JAGP/ECP/contracted	26 + 4 + 4186	−17.25397(10)	0.2330(10)	1.8710(10)	2.583(1)	−0.145(1)	−2.438(1)
JAGP/ECP/hybrid	33 + 724 + 210	−17.25383(4)	0.2308(1)	1.8648(6)	2.5740(7)	−0.1500(7)	−2.4240(7)
JSD/NCP/hybrid	33 + 1086 + 465	−17.20239(5)	0.3303(2)	1.8949(4)	2.5808(5)	−0.1498(5)	−2.4310(5)
JAGP/NCP/hybrid	33 + 724 + 210	−17.20803(6)	0.2786(1)	1.8704(7)	2.5765(8)	−0.1559(8)	−2.4206(8)
JDFT/AE/hybrid	(45) + 1189 + 231	−76.39914(6)	1.1881(3)	1.9152(3)	2.6122(3)	−0.1460(3)	−2.4663(3)
JSD/AE/hybrid	36 + 1038 + 231	−76.40052(5)	1.1579(7)	1.8973(2)	2.5740(3)	−0.1362(3)	−2.4377(3)
JAGP/AE/hybrid	43 + 1163 + 231	−76.40741(2)	1.01531(9)	1.8894(1)	2.5875(1)	−0.1466(1)	−2.4409(1)
method/basis							
MRSD-CI/140CGTO ^d		−76.3963		1.870	2.5556		
HF/aug-cc-pCV6Z ^e				1.9813			
CCSD/aug-cc-pCV6Z ^e				1.8808			
CCSD(T)/aug-cc-pCV6Z ^e				1.8578			
CCSD(T)/CBS ^e				1.858(12)			
experiment^f				1.8546(6)	2.63(2)	−0.13(3)	−2.50(2)

^aFor the quadrupole calculation, the molecule is in the *xy*-plane, with the bisector of the HOH angle parallel to the *y*-axis, and in the reference frame of the center of mass. The VMC expectation values for the dipole and the quadrupole have been calculated as described in Section 3.6. ^bThis column reports the wave function ansatz for the VMC calculations, the description of the two core electrons of the oxygen atom, and the basis set type for the determinantal part. The Jastrow basis is O(4s,2p,1d) H(2s,1p) for the all electrons calculations, and is O(3s,2p,1d) H(2s,1p) for the ECP and NCP cases. Further details in the text. ^cReports the number of parameters for the determinantal basis set, as the summation of the number of exponents (first number, that is written between parentheses in case of *opt:noZ*), number of contraction coefficients (second number, that is zero for uncontracted basis), and the independent elements of the AGP matrix (third number). ^dFrom ref 69. ^eFrom Tables I and VIII of ref 72. ^fDipole from ref 66, quadrupole from ref 67.

these results. Some features were already observed in the previous section; for instance, the advantage of the *opt:all* scheme versus the *opt:noZ* one, and the correlation between energy, variance, and dipole (see Figures S2 and S3 of the Supporting Information).

A selection of the results, representing the largest basis sets (that we can consider at convergence) are reported in Table 1, compared with others highly accurate *ab initio* calculations and the experimental evaluations. Considering both the JSD/ECP and the JAGP/ECP results, with uncontracted, contracted, and hybrid atomic basis, for the basis set convergence the computational advantage of the latter compared with the others can be appreciated. Indeed, calculations with large basis sets are problematic because with the increase of the number of variational parameters a large statistics and computational time are required to obtain a stable optimization. It is therefore crucial to reduce the number of variational parameters in the wave function without missing the important polarization and diffuse terms.

A parallel comparison between similar wave function ansatzes in Table 1 shows that using the ECP pseudopotential leads to lower variances than using NCP pseudopotentials. Following the same trend, the dipoles obtained with ECP are slightly closer to experiments than these calculated using NCP pseudopotentials. In summary, concerning the wave function ansatz, the general trend in accuracy is, as expected,

$$\text{JDFT} < \text{JSD} < \text{JAGPn}^* < \text{JAGP}$$

The JSD wave function has a significant difference in energy and variance with respect to JAGPn* and JAGP, and the quality of the

wave function is also reflected in the accuracy of the dipole moment. We have also observed that, if large basis sets are used, JSD and JDFT are very stable in the optimization, whereas the JAGP wave function requires a larger statistics in the optimization, otherwise it can be unstable.

Comparing the AE versus the ECP or NCP calculations, it emerges that the all electron calculations provide a value for the dipole that is slightly larger than the one obtained with pseudopotentials. The difference could arise from the fact that the basis set convergence in the all electron calculation is more difficult to reach, and to the relativistic effects, that are not considered in the all electron calculations, while are implicitly taken into consideration both in the ECP and in the NCP calculations, through the scalar relativistic correction in the pseudopotentials. According to Lodi et al.,⁷² the relativistic correction to the dipole can be estimated of the order of −0.0043 Deb, that is not enough to completely account for the difference between AE and pseudopotential results, but it is in the right direction.

The accuracy of the VMC evaluations of the dipole appears to be comparable to the CCSD calculations, or better, depending on the wave function ansatz, whereas CCSD(T) calculations with large enough basis (or CBS extrapolation) are closer to the experimental values with respect to our VMC results. For a comparison between the computational and the experimental results, it is important to estimate the order or magnitude of all the theoretical/computational approximations. Beside the already mentioned relativistic effect, there are also the quantum

Table 2. VMC and LRDMC Evaluation of the Ionization Energy (IE) for the Water Molecule, in Comparison with Other Accurate *Ab Initio* Evaluations and Experimental Results^a

method/function/core/opt	$E_{\text{H}_2\text{O}}$ [H]	$E_{\text{H}_2\text{O}^+}$ [H]	IE [eV]
VMC/JSD/ECP/all	−17.2481(1)	−16.7795(1)	12.684(5)
VMC/JAGPn*/ECP/all	−17.2513(1)	−16.7824(1)	12.692(5)
VMC/JAGP/ECP/noZ	−17.2520(1)	−16.7823(1)	12.714(3)
VMC/JAGP/ECP/all	−17.2538(1)	−16.7842(1)	12.711(3)
LRDMC($a \rightarrow 0$)/JAGP/ECP/all	−17.2647(3)	−16.7954(3)	12.703(8)
VMC/JAGP/NCP/noZ	−17.2050(1)	−16.7253(2)	12.986(8)
VMC/JAGP/NCP/all	−17.2068(1)	−16.7383(1)	12.681(3)
VMC/JAGP/AE/noZ	−76.3909(4)	−75.9191(4)	12.771(16)
VMC/JAGP/AE/all	−76.4041(3)	−75.9336(3)	12.736(11)
LRDMC($a \rightarrow 0$)/JAGP/AE/all	−76.4266(1)	−75.9586(2)	12.668(6)
method/basis			
HF/aug-cc-pVQZ ^b			10.868
B3LYP/aug-cc-pVQZ ^b			12.610
MP2FC/aug-cc-pVTZ ^b			12.709
CCSD(T)/aug-cc-pVTZ ^b			12.505
experiment^b			12.621(2)

^aThe ionization energy has been calculated as the sum of the energy difference $\Delta E = E_{\text{H}_2\text{O}} - E_{\text{H}_2\text{O}^+}$ and the zero point energy difference Δ_{ZPE} between the cation and the neutral form of water. For the QMC results, we have considered the Δ_{ZPE} evaluated by a CCSD(T)/aug-cc-pVTZ calculation,⁹⁷ see further details in Section 5.3. ^bFrom ref 97.

nuclei effects. These effects can be accounted by averaging the dipole moment over the ground-state roto-vibrational nuclear-motion, and according to Lodi et al.,⁷² the correction is of the order of +0.0003 Deb, thus rather small. In conclusion, the best VMC description of the dipole moment appears to be provided by the JAGP ansatz, with ECP core and hybrid basis for the determinantal part.

5.3. Ionization and the Atomization Energies. The Ionization Energy (IE) of the water molecule can be estimated from the energy difference $\Delta E = E_{\text{H}_2\text{O}} - E_{\text{H}_2\text{O}^+}$ between the energy $E_{\text{H}_2\text{O}}$ of the neutral molecule H_2O and the energy $E_{\text{H}_2\text{O}^+}$ of the cation H_2O^+ , both in their relaxed geometries. Similarly to the previous section, we have tried several wave function types and several basis, in order to study the basis set convergence. The complete list of the results are reported in the Supporting Information (in Table S7 for the VMC calculations, and in Table S8 for the LRDMC calculations). In Table 2, we report a selection of the results for the largest (more converged) basis sets and a comparison with other *ab initio* calculations and experiments. In order to compare the computational results with the experimentally measured value⁹⁶ $\text{IE}_{\text{exp}} = 12.621(2)$ eV, we have to take into account the difference Δ_{ZPE} between the vibrational zero-point energy (ZPE) of H_2O and of H_2O^+ , which has been estimated by CCSD(T)/aug-cc-pVTZ calculators⁹⁷ to be of the order of 0.067 eV.

We observe in Table 2 that the basis set convergence plays an important role in determining an accurate value for the IE, and also here, the *opt:all* scheme gives a remarkable improvement compared with the *opt:noZ* results. The IE obtained from the VMC approach with all electron calculations is slightly larger than the result for the pseudopotentials. This is probably in part due to the difficulty in reaching the basis set convergence.

The LRDMC results for JAGP function with ECP pseudopotential, yields a minimal improvement compared to the corresponding VMC result. This is a good indication of the high quality of our variational ansatz in the description of the electronic properties of the molecules. In Figure 2 it also appears

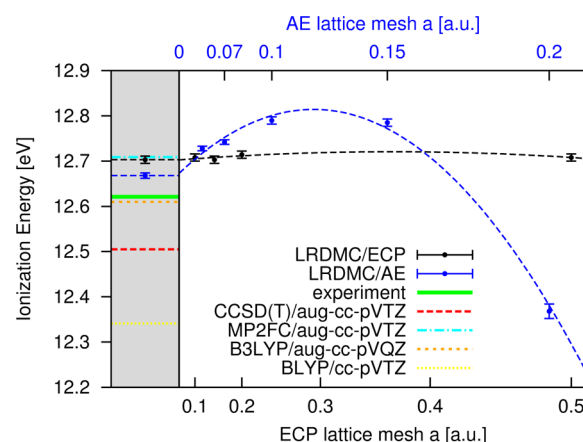


Figure 2. LRDMC evaluation of the ionization energy of the water molecule. Two JAGP wave functions are considered: one corresponding to an all electrons calculation (in blue) and one with ECP pseudopotential for the two core electrons of the oxygen atom (in black). In the right panel, the extrapolation for the lattice mesh $a \rightarrow 0$ is shown, with a functional form $y = c_0 + c_1 a^2 + c_2 a^4$ for the fitted lines; see ref 14. In the left panel with gray background, the LRDMC($a \rightarrow 0$) results are compared with other accurate *ab initio* computational methods and the experimental value.

that the IE for the LRDMC(a) is almost independent of the lattice size a , although the total energy calculated for the different a have a sizable dependence on a (see Supporting Information, Table S8). This consideration can be useful for energy differences estimation, because a LRDMC calculation with $a = 0.5$ is about 25 times computationally cheaper than the one with $a = 0.1$.

The situation for the AE calculation is rather different. First, we have to consider very small values of the lattice size a , otherwise the results are meaningless. Moreover, we observe a large dependence of the IE on the mesh size a . In Figure 2, we also observe that the extrapolated $a \rightarrow 0$ value of the IE is quite close to the experimental value.

Table 3. Atomization Energy of the Water Molecule^a

	$E_{\text{H}_2\text{O}}$ [H]	E_{O} [H]	AE [H]
VMC Calculation/ECP Core/Uncontracted Determinantal Basis ^b			
JSD	−17.24819(5)	−15.87586(9)	0.3723(1)
JAGP	−17.2536(2)	−15.8811(1)	0.3725(2)
$E_{\text{JAGP}} - E_{\text{JSD}}$	0.0054(2)	0.0052(1)	
VMC Calculation/ECP Core/Hybrid Determinantal Basis ^c			
JSD	−17.2471(1)	−15.8769(1)	0.3702(2)
JAGP	−17.25383(4)	−15.8838(2)	0.3700(2)
$E_{\text{JAGP}} - E_{\text{JSD}}$	0.0067(1)	0.0069(2)	
exact ^d	−76.438	−75.0673	0.3707

^aThe atomization energy (AE) is calculated as $E_{\text{H}_2\text{O}} - (E_{\text{O}} + 2E_{\text{H}})$ for different wave functions and basis sets. The hydrogen atom energy E_{H} is 0.5H, with a negligible stochastic error. ^bDeterminantal basis: O(4s,5p,1d) H(3s,1p). Jastrow basis: O(3s,2p,1d) H(2s,2p). ^cDeterminantal basis: O(9s,9p,2d,1f)/{12} H(6s,5p,1d)/{4}. Jastrow basis: O(3s,2p,1d) H(2s,1p). ^dAll electron evaluation of $E_{\text{H}_2\text{O}}$ from ref 69 and of E_{O} from ref 98.

In Table 3 we have reported some VMC estimations of the atomization energy of the water molecule, which has been calculated as $E_{\text{H}_2\text{O}} - (E_{\text{O}} + 2E_{\text{H}})$. More precisely, we considered the JSD and the JAGP ansatzes for two different basis sets: the contracted hybrid basis O(9s,9p,2d,1f)/{12} H(6s,5p,1d)/{4}, with Jastrow basis O(3s,2p,1d) H(2s,1p) and the completely uncontracted basis O(4s,5p,1d) H(3s,1p) with Jastrow O(3s,2p,1d) H(2s,2p). In the calculation, the oxygen atom has been considered in its triplet ground state, whereas the hydrogen energy E_{H} has been set to the exact 0.5H value. All the VMC estimations are in good agreement with the exact value of the atomization energy. It is interesting to note that the JAGP and the JSD estimations are almost identical, whereas there is a small difference, of the order of 2mH, between the estimations of the two different basis. The improvement, in terms of variational energy, from JSD to JAGP, both for the water molecule and for the oxygen atom, is ~6mH, but the fact that JSD and JAGP give

the same atomization energy indicates that this improvement is due only to a better description of the oxygen atom by the JAGP. However, this does not imply that going from JSD to JAGP produces just a vertical shift of the energy and that they provide an equivalent description of the molecular bonds. A better description of the oxygen atom could turn out to an improvement in the description of the OH bond in water and, consequently, of the potential energy surface. In the following sections, we will see that this is actually the case, as JAGP yields an equilibrium structure and vibrational frequencies that appears more accurate than the JSD ones.

5.4. PES Properties: Equilibrium Structure, Harmonic and Fundamental Frequencies. The equilibrium structure and the vibrational frequencies, both harmonic and fundamental, have been calculated for several wave function types and with increasing basis sets. The results that come from the fitting of the energies or of the forces (see Section 4), for all the tested wave functions, are reported in the Table S9 of the Supporting Information. In Table 4 and in Figure 3, we report a selection of the results obtained for the largest basis sets.

In agreement with Zen et al.,⁵¹ we observe that the stochastic error for the minimum energy configuration and the frequencies obtained by the fit of the forces are much smaller than that coming from the fit of the energies. We have also tested the correlated sampling (CS) technique for the fitting of the energies, and, in this case, the error is not much larger than the corresponding one obtained with the force fit. Moreover, we can observe in Table S9 that the results for the JDFT with ECP pseudopotential, obtained by the fitting of the CS energies are not in perfect agreement with the results coming from the fit of the forces. The reason for this discrepancy is easily understood if we consider that, in the expression used for the forces, we are neglecting the explicit derivatives of the parameters, because they vanish at the minimum, as explained in Section 3.4. For a JDFT wave function, this assumption is not correct, because only the parameters in the Jastrow are optimized, whereas the parameters in the determinant remain those of a DFT calculation, and are, in general, not at the minimum of the VMC energy. As a confirmation of this interpretation, we observe that the results for the JSD function with ECP pseudopotential obtained by

Table 4. VMC Evaluation of the Equilibrium Configuration, the Harmonic and the Fundamental Frequencies of the Water Molecule, Compared with Other Accurate *Ab Initio* Evaluations and Experimental Results^a

function/core	equilibrium structure		harmonic freq. [cm ^{−1}]			fundamental freq. [cm ^{−1}]		
	r_0 [Å]	ϕ_0 [deg]	ω_2	ω_1	ω_3	ν_2 [010]	ν_1 [100]	ν_3 [001]
JDFTECP	0.95497(3)	104.49(2)	1664(2)	3882(2)	3995(3)	1610(1)	3693(2)	3787(3)
JSD/ECP	0.95426(3)	104.74(1)	1670(2)	3892(3)	4006(3)	1617(1)	3702(3)	3794(2)
JAGPn*/ECP	0.95612(8)	104.17(2)	1710(3)	3896(6)	3990(7)	1654(1)	3710(3)	3800(7)
JAGP/ECP	0.95550(4)	104.41(1)	1669(1)	3872(3)	3974(4)	1613.3(6)	3677(2)	3772(2)
JSD/NCP	0.95536(3)	104.85(1)	1668(2)	3889(2)	4001(3)	1613.1(9)	3700(2)	3796(3)
JAGP/NCP	0.95668(3)	104.52(1)	1663(2)	3869(2)	3973(3)	1610.4(7)	3679(2)	3767(3)
method/basis								
BLYP/aug-cc-pVTZ ^b	0.9719	104.47	1596	3655	3757	1543	3480	3567
B3LYP/aug-cc-pVTZ ^b	0.9619	105.08	1627	3796	3899	1575	3631	3720
FC MP2/aug-cc-pVTZ ^b	0.9614	104.11	1628	3822	3948	1578	3653	3767
CISD/(13,8,4,2/8,4,2) ^c	0.952	104.8	1676.1	3947.3	4050.5			
CCSD/(13,8,4,2/8,4,2) ^c	0.956	104.4	1662.5	3870.9	3977.8			
FC CCSD(T)/aug-cc-pV7Z ^d	0.95831	104.452	1649.83	3835.55	3946.05	1595.58	3659.31	3757.45
experiment ^e	0.95721(30)	104.522(50)	1648.47	3832.17	3942.53	1594.59	3656.65	3755.79

^aFor the VMC results, the equilibrium configuration, the harmonic frequencies ω_i and the fundamental frequencies ν_i have been evaluated from the PES fitted using the VMC forces; see details in the text and in Zen et al.⁵¹ ^bFrom ref 99. ^cFrom ref 74. ^dFrom ref 75. ^eFrom ref 68.

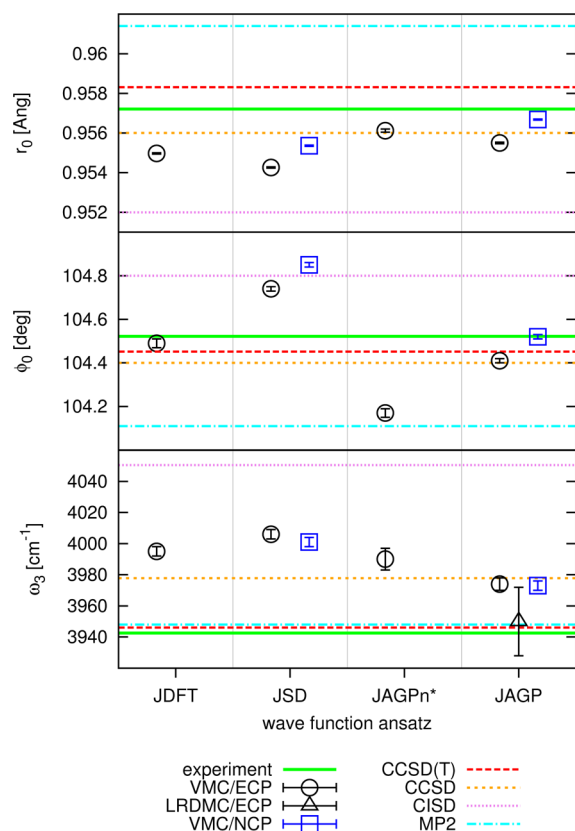


Figure 3. Following properties of the ground state PES of the water molecule around the equilibrium structure are reported: the bond length r_0 , the bond angle ϕ_0 , and the harmonic frequency of the asymmetric stretching ω_3 . VMC results for JDFT, JSD, JAGPn*, and JAGP wave functions are reported, using ECP (in black) and NCP (in blue) pseudopotential for the two core electrons of the oxygen. The LRDMC ($a \rightarrow 0$) value of ω_3 for the JAGP/ECP function extrapolated in Figure 5 is also shown. For a comparison, the results of MP2, CISD, CCSD, and CCSD(T) calculations are reported (see Table 4 and references therein for details).

fitting of the CS energies and of the forces are compatible within the estimated stochastic errors.

It is evident that the equilibrium structure and the frequencies are clearly and smoothly converging with an increasing basis set, and both the *opt:all* and the hybrid atomic orbitals are very useful for this convergence. The converged equilibrium structure is in good agreement both with other highly accurate *ab initio* calculations and with the experimental values, also reported in Table 4. The calculated frequencies are slightly overestimated compared with the experimental results of the CCSD(T) values, but they are in agreement with the CCSD results.

By comparing the JSD and the JAGP results (with the larger basis sets), we notice that the latter ones are closer to the experimental values, see Figure 3. This is an indication that the JAGP ansatz provides a better description of the PES and of the chemical bonds, as compared with the JSD ansatz.

Converged results obtained using ECP or NCP are in good agreement for the frequencies, while it appears that the OH bond for the equilibrium structure obtained from ECP is slightly smaller than the bond for NCP. This leads us to ask which pseudopotential is more compatible with the all-electron calculations, either ECP or NCP. Since all-electron calculations are computationally expensive, especially if we consider a basis that is large enough to be considered converged, we have decided

to address this question by simply evaluating the residual force in the experimental equilibrium configuration with both pseudo-potentials. As can be observed from Figure 4, the ECP pseudopotential is more compatible with the AE calculations.

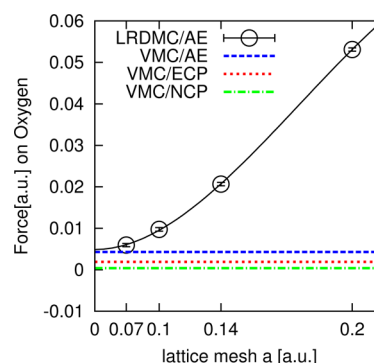


Figure 4. Residual force (in H/Bohr) on the oxygen atom, calculated on the experimental equilibrium structure. The reported values correspond to VMC calculations with AE (blue), ECP (red) or NCP (green) core, and LRDMC calculations (black) with AE core and lattice mesh size a equal to 0.07, 0.1, 0.14, and 0.2 Bohr. The fitting line $F = f_0 + f_1 a^2 + f_2 a^4$ for the LRDMC calculations is reported in black.

It is clear that, by comparing the VMC frequencies with the experimental or the CCSD(T) ones, there is still room to improve the accuracy of the QMC variational wave function as far as the vibrational properties are concerned. We have explored the possibility to go beyond the variational scheme using LRDMC calculations. Since these calculations are much more computationally demanding than VMC, we have only evaluated at the LRDMC level the frequency of vibration of the asymmetric stretching of the molecule by interpolating the one-dimensional energy profile computed along the mode eigenvector (computed by the VMC/JAGP/ECP). The analysis of different mesh sizes a , together with the corresponding harmonic frequencies ω_3 are reported in Figure 5(a). The interpolating lines have been used to extrapolate an estimation of the frequency and are reported in Figure 5(b) and in Table S10 of the Supporting Information.

Figure 5(b) shows for the LRDMC estimates a general improvement in the value of the frequency, from the VMC $\omega_3^{\text{VMC}} = 3989(9)$ cm⁻¹ toward the experimental value $\omega_3^{\text{exp}} = 3942.53$ cm⁻¹, because the LRDMC $a \rightarrow 0$ extrapolation $\omega_3^{a \rightarrow 0} = 3950(22)$ cm⁻¹ differs from ω_3^{exp} only by ~ 7 cm⁻¹, that is, within 1 σ . Therefore, the size of the stochastic error does not allow to definitively conclude that LRDMC, within the fixed node approximation, provides a very accurate frequency, but it is likely that it improves the VMC calculations. To definitely solve this issue, it is necessary to further decrease the stochastic error, which is at least 1 order of magnitude computationally more expensive than the corresponding VMC calculations. Moreover, we have seen that we need a careful $a \rightarrow 0$ extrapolation, with almost prohibitive computations with small a values. It could be that, always within the fixed node approximation, the DMC approach gives more accurate results. However, the most convenient way to enhance the precision of the frequency estimation for a fixed node calculation is probably to use the forces, as for our VMC calculations. To this aim several other issues have to be tackled, such as having a consistent estimation of the force with finite variance and eliminating any possible bias due to the mesh size a for LRDMC or to the time step τ for DMC.

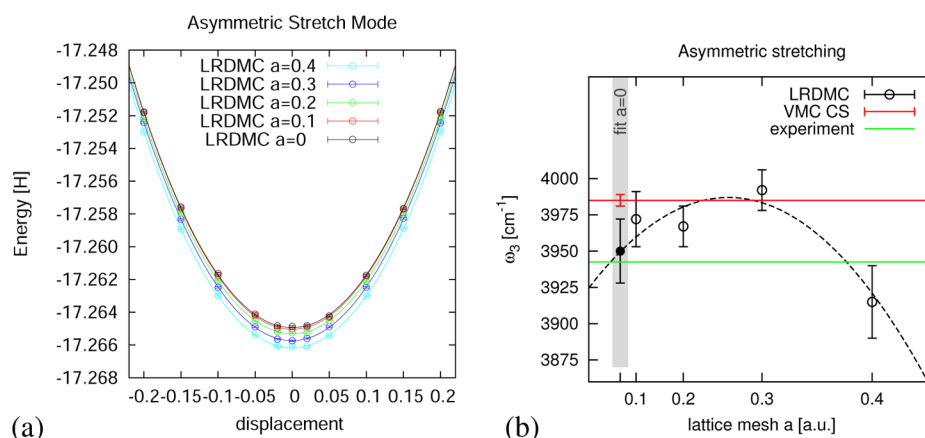


Figure 5. We consider a JAGP/ECP wave function. In panel (a) we report the LRDMC values of energy, calculated for lattice mesh sizes a of 0.4, 0.3, 0.2, 0.1, and extrapolation to zero. The displacement is along the asymmetric stretching mode, and the center corresponds to the VMC minimum structure for this wave function. The fitting functions $y(x) = c_0 + c_2x^2 + c_4x^4$ are represented in the plot as color coded continuous lines. In panel (b) the values for the harmonic frequency are reported versus the corresponding values of the lattice mesh a . For a comparison, the experimental evaluation and the value obtained from the correlated sampling of the VMC energies is also shown, in green and red, respectively.

6. CONCLUSIONS

In this paper, we have considered the water molecule as a test system to challenge the abilities of QMC approaches to evaluate several molecular properties: the energy, the dipole and the quadrupole momenta, the ionization and the atomization energies, the structural minimum, and the harmonic and fundamental frequencies of vibrations. For each of these quantities, we have performed and compared several calculations corresponding to different setups for the QMC algorithm, namely: different ansatzes, different basis sets and contraction schemes, different ways to tackle the core electrons. Most of the investigation reported are based on VMC calculations, but we have also carried out several LRDMC calculations in order to go beyond the variational ansatz.

It is known^{33,53,54,65,100,101} that the accuracy of QMC evaluations, both in the variational and diffusion approaches, strongly depends on the wave function ansatz. However, systematic studies on the differences between the various ansatzes are typically limited to the total energy evaluation, whereas molecular properties can be more sensitive to these choices. Here, we have compared the JDFT, JSD, JAGPn*, and JAGP ansatzes versus a larger set of properties, always bearing in mind that a good ansatz has to provide reliable results using a compact wave function with a limited number of variational parameters. This is important, because the optimization of the wave function could otherwise be difficult, especially if large molecules and large basis sets are taken into consideration.

In the first part of our work, we focused on the study of the basis set convergence, underlining the importance to optimize also the exponents of the orbitals in order to have a better chemical description with a lower number of parameters. Inspired by the strong interplay between the building of the AGP wave function and the atomic orbitals, we have introduced a new kind of orbital contraction that we have termed atomic hybrid orbitals, which are specifically constructed for QMC calculations and are somehow similar to the natural hybrid orbitals expansion.⁷⁷ In particular, the atomic hybrid orbitals allow us to introduce diffuse and polarization orbitals in the wave function, with an impact in terms of number of parameters much lower than the one introduced by ordinary contracted or uncontracted orbitals. Even if orbital exponents are optimized, a converged basis set for the molecular properties, such as dipole

and vibrational frequencies, requires the presence of diffuse and polarization orbitals. Atomic hybrid orbitals result therefore in a remarkable computational advantage, especially for large systems. According to our observations, it emerges that the JAGP ansatz with hybrid orbitals represents the best balance between accuracy of the results and compactness of the wave function. The reduced number of variational parameters allows us an easy management of the wave function optimization procedure, and opens perspectives for the application of VMC to large molecules using large basis sets.

We have also considered the impact of the description of the core electrons of the oxygen by energy consistent ECP⁹¹ and norm conserving NCP⁹² pseudopotentials, versus an all electron AE calculation. Although some differences between these three approaches were observed, we have noticed that for converged basis the differences are quite small and they reach almost the same level of accuracy. Thus, the most convenient choice seems the ECP, because it is computationally cheaper than AE, and it gives *ceteris paribus* a smaller variance with respect to NCP.

The LRDMC calculations reported in this work demonstrate that the projection schemes with fixed node approximation can partly improve the VMC results, although the computational cost is often high. This confirms the quality of the JAGP wave function, not only for the description of the electronic properties of relaxed molecules but also of forces and potential energy surfaces. On the other hand, projection methods are computationally more demanding, and as we have seen, often they are limited by a very difficult and expensive extrapolation to the continuous limit $a \rightarrow 0$ (that is the analogous of the extrapolation of the time step $\tau \rightarrow 0$ for the DMC). In conclusion, the use of the JAGP wave function in combination with the hybrid orbital contraction scheme represents a promising way for an accurate many body calculation of properties for large molecules.

■ ASSOCIATED CONTENT

Supporting Information

Description of the optimization schemes of the different wave function ansatzes; several tables, with the details about the considered basis sets; the complete list of the results for all the studied wave functions, whose in this manuscript we have reported only a selection; three supporting figures, showing the basis set convergence for the energies, the variances, and the

dipoles. This material is available free of charge via the Internet at <http://pubs.acs.org/>.

AUTHOR INFORMATION

Corresponding Authors

*E-mail: sorella@sisssa.it.

*E-mail: leonardo.guidoni@univaq.it.

Notes

The authors declare no competing financial interest.

ACKNOWLEDGMENTS

The authors thank Michele Casula for useful comments and Matteo Barborini for illuminating discussions and critical reading of the manuscript. The authors acknowledge funding provided by the European Research Council project no. 240624 within the VII Framework Program of the European Union and by MIUR within PRIN 2011 project. Computational resources were supplied by CINECA (ISCRA award no. HP10AOW1FU), PRACE infrastructure, and the Caliban-HPC centre at the Università de L'Aquila.

REFERENCES

- (1) Austin, B. M.; Zubarev, D. Y.; Lester, W. A. J. *Chem. Rev.* **2012**, *112*, 263–288.
- (2) Needs, R. J.; Towler, M. D.; Drummond, N. D.; Rios, P. L. *J. Phys.: Condens. Matter* **2010**, *22*, 023201.
- (3) Assaraf, R.; Caffarel, M.; Khelif, A. *J. Phys. A: Math. Theor.* **2007**, *40*, 1181–1214.
- (4) Foulkes, W. M. C.; Mitás, L.; Needs, R. J.; Rajagopal, G. *Rev. Mod. Phys.* **2001**, *73*, 33–83.
- (5) Reynolds, P. J.; Ceperley, D. M.; Alder, B. J.; Lester, W. A. J. *Chem. Phys.* **1982**, *77*, 5593–5603.
- (6) DePasquale, M. F.; Rothstein, S. M.; Vrbik, J. J. *Chem. Phys.* **1988**, *89*, 3629.
- (7) Umrigar, C. J.; Nightingale, M. P.; Runge, K. J. *J. Chem. Phys.* **1993**, *99*, 2865–2890.
- (8) Mitás, L.; Shirley, E. L.; Ceperley, D. M. *J. Chem. Phys.* **1991**, *95*, 3467.
- (9) Kalos, M. *Phys. Rev.* **1962**, *128*, 1791–1795.
- (10) Trivedi, N.; Ceperley, D. *Phys. Rev. B* **1990**, *41*, 4552–4569.
- (11) Buonaura, M.; Sorella, S. *Phys. Rev. B* **1998**, *57*, 11446–11456.
- (12) Sorella, S.; Capriotti, L. *Phys. Rev. B* **2000**, *61*, 2599–2612.
- (13) Casula, M.; Filippi, C.; Sorella, S. *Phys. Rev. Lett.* **2005**, *95*, 100201.
- (14) Casula, M.; Moroni, S.; Sorella, S.; Filippi, C. *J. Chem. Phys.* **2010**, *132*, 154113.
- (15) Al-Saidi, W. A.; Zhang, S.; Krakauer, H. J. *Chem. Phys.* **2006**, *124*, 224101.
- (16) Zhang, S.; Krakauer, H. *Phys. Rev. Lett.* **2003**, *90*, 136401.
- (17) Baer, R.; Head-Gordon, M.; Neuhauser, D. *J. Chem. Phys.* **1998**, *109*, 6219.
- (18) Chen, B.; Anderson, J. B. *J. Chem. Phys.* **1995**, *102*, 4491.
- (19) Ceperley, D. M.; Alder, B. J. *J. Chem. Phys.* **1984**, *81*, 5833.
- (20) Bajdich, M.; Tiago, M. L.; Hood, R. Q.; Kent, P. R. C.; Reboredo, F. A. *Phys. Rev. Lett.* **2010**, *104*, 193001.
- (21) Baroni, S.; Moroni, S. *Phys. Rev. Lett.* **1999**, *82*, 4745–4748.
- (22) Yuen, W. K.; Oblinsky, D. G.; Giacometti, R. D.; Rothstein, S. M. *Int. J. Quantum Chem.* **2009**, *109*, 3229–3234.
- (23) Booth, G. H.; Thom, A. J. W.; Alavi, A. J. *Chem. Phys.* **2009**, *131*, 054106.
- (24) Coccia, E.; Guidoni, L. *J. Comput. Chem.* **2012**, *33*, 2332–2339.
- (25) Barborini, M.; Sorella, S.; Guidoni, L. *J. Chem. Theory Comput.* **2012**, *8*, 1260–1269.
- (26) Filippi, C.; Buda, F.; Guidoni, L.; Sinicropi, A. J. *Chem. Theory Comput.* **2012**, *8*, 112–124.
- (27) Kolorenc, J.; Mitás, L. *Rep. Prog. Phys.* **2011**, *74*, 026502.
- (28) Maezono, R.; Drummond, N. D.; Ma, A.; Needs, R. J. *Phys. Rev. B* **2010**, *82*, 184108.
- (29) Valsson, O.; Filippi, C. *J. Chem. Theory Comput.* **2010**, *6*, 1275–1292.
- (30) Spanu, L.; Sorella, S.; Galli, G. *Phys. Rev. Lett.* **2009**, *103*, 196401.
- (31) Zimmerman, P. M.; Toulouse, J.; Zhang, Z.; Musgrave, C. B.; Umrigar, C. J. *J. Chem. Phys.* **2009**, *131*, 124103.
- (32) Sterpone, F.; Spanu, L.; Ferraro, L.; Sorella, S.; Guidoni, L. *J. Chem. Theory Comput.* **2008**, *4*, 1428–1434.
- (33) Sorella, S.; Casula, M.; Rocca, D. J. *Chem. Phys.* **2007**, *127*, 014105.
- (34) Schautz, F.; Filippi, C. *J. Chem. Phys.* **2004**, *120*, 10931–10941.
- (35) Caffarel, M.; Rerat, M.; Pouchan, C. *Phys. Rev. A* **1993**, *47*, 3704–3717.
- (36) Bartlett, R.; Musiat, M. *Rev. Mod. Phys.* **2007**, *79*, 291–352.
- (37) Sherrill, C. D.; Schaefer, H. F., III *The Configuration Interaction Method: Advances in Highly Correlated Approaches*; Elsevier: Amsterdam, 1999; pp 143–269.
- (38) Möller, C.; Plesset, M. S. *Phys. Rev.* **1934**, *46*, 618–622.
- (39) Head-Gordon, M.; Pople, J. A.; Frisch, M. J. *Chem. Phys. Lett.* **1988**, *153*, 503–506.
- (40) Filippi, C.; Umrigar, C. J. *Phys. Rev. B* **2000**, *61*, R16291–R16294.
- (41) Umrigar, C. J. *Int. J. Quantum Chem.* **1989**, 217–230.
- (42) Assaraf, R.; Caffarel, M. J. *Chem. Phys.* **2000**, *113*, 4028–4034.
- (43) Assaraf, R.; Caffarel, M. J. *Chem. Phys.* **2003**, *119*, 10536–10552.
- (44) Attaccalite, C.; Sorella, S. *Phys. Rev. Lett.* **2008**, *100*, 114501.
- (45) Sorella, S.; Capriotti, L. J. *Chem. Phys.* **2010**, *133*, 234111.
- (46) Chiesa, S.; Ceperley, D. M.; Zhang, S. *Phys. Rev. Lett.* **2005**, *94*, 036404.
- (47) Wagner, L. K.; Grossman, J. C. *Phys. Rev. Lett.* **2010**, *104*, 210201.
- (48) Barborini, M.; Guidoni, L. *J. Chem. Phys.* **2012**, *137*, 224309.
- (49) Coccia, E.; Varsano, D.; Guidoni, L. *J. Chem. Theory Comput.* **2013**, *9*, 8–12.
- (50) Coccia, E.; Chernomor, O.; Barborini, M.; Sorella, S.; Guidoni, L. *J. Chem. Theory Comput.* **2012**, *8*, 1952–1962.
- (51) Zen, A.; Zhelyazov, D.; Guidoni, L. *J. Chem. Theory Comput.* **2012**, *8*, 4204–4215.
- (52) Umrigar, C. J.; Toulouse, J.; Filippi, C.; Sorella, S.; Hennig, R. G. *Phys. Rev. Lett.* **2007**, *98*, 110201.
- (53) Clark, B. K.; Morales, M. A.; McMinis, J.; Kim, J.; Scuseria, G. E. *J. Chem. Phys.* **2011**, *135*, 244105.
- (54) Morales, M. A.; McMinis, J.; Clark, B. K.; Kim, J.; Scuseria, G. E. *J. Chem. Theory Comput.* **2012**, *8*, 2181–2188.
- (55) Xu, J.; Deible, M. J.; Peterson, K. A.; Jordan, K. D. *J. Chem. Theory Comput.* **2013**, *9*, 2170–2178.
- (56) Jastrow, R. *Phys. Rev.* **1955**, *98*, 1479–1484.
- (57) Casula, M.; Sorella, S. *J. Chem. Phys.* **2003**, *119*, 6500–6511.
- (58) Bajdich, M.; Mitás, L.; Wagner, L. K.; Schmidt, K. E. *Phys. Rev. B* **2008**, *77*, 115112.
- (59) Bajdich, M.; Mitás, L.; Drobný, G.; Wagner, L.; Schmidt, K. *Phys. Rev. Lett.* **2006**, *96*, 130201.
- (60) Holzmann, M.; Ceperley, D. M.; Pierleoni, C.; Esler, K. *Phys. Rev. E* **2003**, *68*, 046707.
- (61) Toulouse, J.; Umrigar, C. J. *J. Chem. Phys.* **2008**, *128*, 174101.
- (62) Fracchia, F.; Filippi, C.; Amovilli, C. *J. Chem. Theory Comput.* **2012**, *8*, 1943–1951.
- (63) Neuscamman, E. *Phys. Rev. Lett.* **2012**, *109*, 203001.
- (64) Petruziello, F. R.; Toulouse, J.; Umrigar, C. J. *J. Chem. Phys.* **2011**, *134*, 064104.
- (65) Marchi, M.; Azadi, S.; Casula, M.; Sorella, S. *J. Chem. Phys.* **2009**, *131*, 154116.
- (66) Clough, S. A.; Beers, Y.; Klein, G. P.; Rothman, L. S. *J. Chem. Phys.* **1973**, *59*, 2254.
- (67) Verhoeven, J.; Dymanus, A. J. *Chem. Phys.* **1970**, *52*, 3222.
- (68) Benedict, W. S.; Gailar, N.; Plyler, E. K. *J. Chem. Phys.* **1956**, *24*, 1139–1165.
- (69) Feller, D.; Boyle, C. M.; Davidson, E. R. *J. Chem. Phys.* **1987**, *86*, 3424.
- (70) Partridge, H.; Schwenke, D. J. *Chem. Phys.* **1997**, *106*, 4618–4639.
- (71) Schwenke, D. W.; Partridge, H. *J. Chem. Phys.* **2000**, *113*, 6592.

- (72) Lodi, L.; Tolchenov, R. N.; Tennyson, J.; Lynas-Gray, A. E.; Shirin, S. V.; Zobov, N. F.; Polyansky, O. L.; Csaszar, A. G.; van Stralen, J. N. P.; Visscher, L. *J. Chem. Phys.* **2008**, *128*, 044304.
- (73) Csaszar, A. G.; Czako, G.; Furtenbacher, T.; Tennyson, J.; Szalay, V.; Shirin, S. V.; Zobov, N. F.; Polyansky, O. L. *J. Chem. Phys.* **2005**, *122*, 214305.
- (74) Kim, J. S.; Lee, J. Y.; Lee, S.; Mhin, B. J.; Kim, K. S. *J. Chem. Phys.* **1995**, *102*, 310–317.
- (75) Feller, D.; Peterson, K. A. *J. Chem. Phys.* **2009**, *131*, 154306.
- (76) Kato, T. *Commun. Pure Appl. Math.* **1957**, *10*, 151–177.
- (77) Foster, J. P.; Weinhold, F. *J. Am. Chem. Soc.* **1980**, *102*, 7211.
- (78) Hurley, A. C.; Lennard-Jones, J.; Pople, J. A. *Proc. R. Soc. London, Ser. A* **1953**, *220*, 446–455.
- (79) Coleman, A. J. *J. Math. Phys.* **1972**, *13*, 214–222.
- (80) Casula, M.; Attaccalite, C.; Sorella, S. *J. Chem. Phys.* **2004**, *121*, 7110–7126.
- (81) Filippi, C.; Umrigar, C. J. *J. Chem. Phys.* **1996**, *105*, 213–226.
- (82) Trail, J. R. *Phys. Rev. E* **2008**, *77*, 016703.
- (83) Kunsch, H. R. *Ann. Stat.* **1989**, *17*, 1217–1241.
- (84) Wolff, U. *Comput. Phys. Commun.* **2004**, *156*, 143–153.
- (85) Sorella, S. *Phys. Rev. B* **2005**, *71*, 241103.
- (86) Toulouse, J.; Umrigar, C. J. *J. Chem. Phys.* **2007**, *126*, 084102.
- (87) Sorella, S. In *Variational Monte Carlo and Markov Chains for Computational Physics*; Avella, A., Mancini, F., Eds.; Springer: Berlin/Heidelberg, 2013; pp 207–236.
- (88) Mazzola, G.; Zen, A.; Sorella, S. *J. Chem. Phys.* **2012**, *137*, 134112.
- (89) Assaraf, R.; Caffarel, M.; Scemama, A. *Phys. Rev. E* **2007**, *75*, 035701.
- (90) Sorella, S. *TurboRVB* Quantum Monte Carlo package. <http://people.sissa.it/~sorella/web/index.html> (accessed Nov. 1, 2012).
- (91) Burkatzki, M.; Filippi, C.; Dolg, M. *J. Chem. Phys.* **2007**, *126*, 234105.
- (92) Trail, J.; Needs, R. *J. Chem. Phys.* **2005**, *122*, 174109.
- (93) Azadi, S.; Cavazzoni, C.; Sorella, S. *Phys. Rev. B* **2010**, *82*, 125112.
- (94) Dunning, T. H. *J. Chem. Phys.* **1989**, *90*, 1007–1023.
- (95) Kendall, R.; Dunning, T.; Harrison, R. *J. Chem. Phys.* **1992**, *96*, 6796–6806.
- (96) NIST Chemistry Webbook. <http://webbook.nist.gov/chemistry> (accessed March 2013).
- (97) Computational Chemistry Comparison and Benchmark Database. <http://cccbdb.nist.gov/> (accessed March 2013).
- (98) Chakravorty, S.; Gwaltney, S.; Davidson, E.; Parpia, F.; p Fischer, C. *Phys. Rev. A* **1993**, *47*, 3649–3670.
- (99) Barone, V. *J. Chem. Phys.* **2005**, *122*, 014108.
- (100) Brown, M. D.; Trail, J. R.; Rios, P. L.; Needs, R. J. *J. Chem. Phys.* **2007**, *126*, 224110.
- (101) Lopez Rios, P.; Seth, P.; Drummond, N. D.; Needs, R. J. *Phys. Rev. E* **2012**, *86*, 036703.